POLITECNICO DI MILANO

Dipartimento di Elettronica, Informazione e Bioingegneria

Corso di Laurea Magistrale in Biomedical Engineering

LONGITUDINAL QUANTITATIVE SUSCEPTIBILITY MAPPING INVESTIGATION OF THE NORMAL - APPEARING WHITE MATTER IN MULTIPLE SCLEROSIS

Relatore: Prof.ssa Anna Maria BIANCHI

Correlatore: Ing. Valeria Elisa CONTARINO

Tesi di Laurea di:

Aurelia MORABITO

Matr. 921373

Ringraziamenti

Abstract

The multiple sclerosis is an autoimmune inflammatory chronic disease of the central nervous system characterized by the loss of motor and sensory function, whose diagnosis involves an integration of clinical, laboratory and radiographic data.

The white matter lesions are a pathological landmark of the disease and a very sensitive point of reference for its diagnosis. However, scientific literature has proven that abnormalities in multiple sclerosis patients are present even in the regions of the white matter that appear radiologically normal, which are referred as *normal-appearing white matter* (NAWM).

Alongside this evidence, *Quantitative Susceptibility Mapping* (QSM) has become increasingly prominent to detect tissue changes that occur in multiple sclerosis by quantifying the tissues intrinsic characteristic known as *susceptibility*.

A total of 59 patients were recruited and scanned at 3T magnetic resonance unit of *Fondazione IRCCS Ca' Granda Ospedale Maggiore Policlinico* (Milan). Thirteen of the patients were recruited for a longitudinal study.

Two neuroimaging pipelines have been developed and applied in order to conduct a longitudinal investigation of susceptibility in the normal-appearing white matter and inside the white matter lesions in multiple sclerosis: the first pipeline has been applied separately for two time point groups (G0 and G1), comprising different patients whose magnetic resonance was acquired respectively within 6 months and after more than 6 months their diagnosis of multiple sclerosis; the second pipeline has been applied to a subgroup of patients whose magnetic resonance was available at both time points (T0 and T1). For this longitudinal study group, an evaluation of the changes in susceptibility in the lesion areas that decreased/did not change/increased between the two time points was performed as well.

This whole-brain processing included four main steps: *FreeSurfer* automatic segmentation of the brain, automatic segmentation of the WM lesions with the *Lesion Growth Algorithm* (LGA) of the *Lesion Segmentation Tool* (LST), QSM processing through the *Matlab*

toolbox *STI Suite* and, for the longitudinal study group, lesion change detection by the *longitudinal pipeline* of the *Lesion Segmentation Tool* (LST).

The extracted neuroimaging measurements were the mean value of susceptibility in the regions of interest and the volume of different cerebral structures. In particular, the mean value of susceptibility was assessed in the NAWM, inside the WM lesions and inside the decreased/not changed/increased lesion areas of the longitudinal study group, whereas the volume was evaluated for the NAWM, the WM, the GM, the CSF and the whole intracranial matter (TIV).
Clinical information regarding the MS phenotype, the degree of disability quantified by the *Expanded Disability Status Scale* (EDSS) score and the disease duration was also integrated in the analysis.

The conducted statistical tests were chi-squared tests to assess group differences in sex, Mann-Whitney tests to perform age and disease duration comparison between groups, Mann-Whitney tests and Wilcoxon tests to perform a univariate comparison of the neuroimaging measurements, Spearman's tests to look for correlations between neuroimaging measurements and clinical variables, multiple regression models in order to forecast the value of clinical variables (ΔEDSS) and of neuroimaging variables (GMF) by using the mean value of susceptibility in the NAWM as main predictor.

A statistically significant difference in the mean value of susceptibility in the NAWM has been demonstrated between progressive patients and relapsing-remitting patients within group G0 and even more within group G1, suggesting higher and ongoing inflammation and demyelination processes in progressive patients and indicating the mean value of susceptibility in the NAWM as an aid to diagnosis. Statistically significant correlations of the mean value of susceptibility in the NAWM have been found with brain atrophy measurements (NAWMF and GMF) and with disability measurements (ΔEDSS), meaning that this neuroimaging measurement might also have a role in predicting brain atrophy and disability. The latter have been further confirmed by multiple regression models which have predicted the ΔEDSS utilizing the mean value of susceptibility in the NAWM as statistically significant independent variable.
The statistical analysis of the longitudinal study group has corroborated the correlations of the mean value of susceptibility in the NAWM with brain atrophy measurements (GMF)

and disability measurements (ΔEDSS). The former has been supported with multiple regression models which have been able to forecast the GMF at both time points by using the mean value of susceptibility in the NAWM as statistically significant predictor.

The study suggests that QSM is sensitive to tissue characteristics specific to the different time points and phenotypes of MS. On the basis of the evidence of the presented work, larger studies are encouraged to validate the utility of QSM to support diagnosis and to prognosticate the course of the disease. Multi-modal studies on the NAWM are also suggested in order to provide a more complete characterization of the NAWM in MS.

Sommario

La sclerosi multipla è una malattia cronica autoimmune infiammatoria del sistema nervoso centrale caratterizzata dalla perdita di funzioni motorie e sensoriali, la cui diagnosi prevede l'integrazione di dati clinici, radiologici e di laboratorio.

Le lesioni della materia bianca sono un segno distintivo e molto sensibile per la diagnosi di questa malattia. Tuttavia, la letteratura scientifica ha dimostrato che le anormalità nei pazienti affetti da sclerosi multipla sono presenti anche nelle regioni di materia bianca che appaiono radiologicamente normali, che sono chiamate *normal-appearing white matter* (NAWM).

Accanto a queste evidenze, la Quantitative Susceptibility Mapping (QSM) si sta rivelando prominente per rilevare i cambiamenti nei tessuti che avvengono nei pazienti affetti da sclerosi multipla, quantificando la proprietà intrinseca dei tessuti nota come *suscettività*.

Un totale di 59 pazienti è stato reclutato e sottoposto a risonanza magnetica a 3T nel reparto di neuroradiologia della *Fondazione IRCCS Ca' Granda Ospedale Maggiore Policlinico* (Milano). Tredici di questi pazienti sono stati reclutati per uno studio longitudinale.

Due pipeline di neuroimaging sono state implementate e applicate ai fini di condurre un'analisi longitudinale della suscettività nella NAWM e nelle lesioni della materia bianca in pazienti con sclerosi multipla: la prima pipeline è stata applicata separatamente per due gruppi (G0 e G1) comprendenti diversi pazienti la cui risonanza magnetica era stata acquisita rispettivamente entro 6 mesi e dopo più di 6 mesi dalla loro diagnosi di sclerosi multipla; la seconda pipeline è stata applicata al sottogruppo dei pazienti la cui risonanza magnetica era disponibile in entrambi i tempi (T0 e T1). Per questo gruppo di studio longitudinale, è stato condotto anche uno studio sui cambiamenti di suscettività nelle zone delle lesioni che erano guarite/rimaste invariate/comparse tra i due tempi.

Questa elaborazione whole-brain ha incluso quattro passaggi principali: segmentazione automatica dei tessuti cerebrali con *FreeSurfer,* segmentazione automatica delle lesioni

della materia bianca tramite il *Lesion Growth Algorithm* (LGA) del *Lesion Segmentation Tool* (LST), la QSM ottenuta attraverso il toolbox di *Matlab STI Suite* e, per il gruppo di studio longitudinale, il rilevamento dei cambiamenti delle lesioni tramite la *longitudinal pipeline* del *Lesion Segmentation Tool* (LST).

Le misure di neuroimaging estratte sono state il valore medio della suscettività nelle regioni di interesse e il volume dei diversi tessuti cerebrali. In particolare, il valore medio della suscettività è stato valutato nella NAWM, nelle lesioni della materia bianca e nelle zone delle lesioni guarite/invariate/comparse tra i due tempi del gruppo longitudinale, mentre il volume è stato stimato per la NAWM, la WM, la GM, il CSF e l'intera materia intracranica (TIV).
Questi dati sono stati integrati per le successive analisi con informazioni cliniche riguardanti il fenotipo della malattia, il grado di disabilità quantificato tramite l'*Expanded Disability Status Scale* (EDSS) e la durata di malattia.

I test statistici condotti sono stati dei test chi-quadrato per determinare le differenze di sesso tra gruppi, dei test di Mann-Whitney per comparare età e durata di malattia tra gruppi, dei test di Mann-Whitney e di Wilcoxon per svolgere un'analisi univariata delle misure di neuroimaging, dei test di Spearman per individuare le correlazioni tra misure di neuroimaging e variabili cliniche e modelli di regressioni multipla per prevedere il valore di variabili cliniche (ΔEDSS) e di neuroimaging (GMF) usando come predittore principale il valore medio della suscettività nella NAWM.

È stata dimostrata una differenza statisticamente significativa del valore medio di suscettività nella NAWM tra i pazienti progressivi e i pazienti recidivanti-remittenti già per il gruppo G0, che si è rivelata ancora più significativa per il gruppo G1. Questo suggerisce maggiori e correnti processi di infiammazioni e demielinizzazione nei pazienti progressivi rispetto a quelli recidivanti-remittenti e individua il valore medio di suscettività nella NAWM come potenziale misura di supporto alla diagnosi. Correlazioni statisticamente significative per il valore medio di suscettività nella NAWM sono state trovate con misure di atrofia cerebrale (NAWMF e GMF) e con misure di disabilità (ΔEDSS), suggerendo che questa misura di neuroimaging possa avere anche un ruolo nel predire l'atrofia cerebrale e la disabilità. Questo è stato ulteriormente confermato da due modelli di regressione multipla in cui il valore medio della suscettività nella NAWM è stato impiegato come

variabile indipendente statisticamente significativa per predire la Grey Matter Fraction (GMF).

L'analisi statistica per il gruppo di studio longitudinale ha corroborato la correlazione del valore medio di suscettività nella NAWM con misure di atrofia cerebrale (GMF) e disabilità (ΔEDSS). La prima correlazione è stata supportata con un modello di regressione multipla che è stato in grado di predire la GMF in entrambi i tempi usando il valore medio di suscettività nella NAWM come predittore statisticamente significativo.

Lo studio suggerisce come la QSM sia uno strumento sensibile alle caratteristiche specifiche dei tessuti in diversi time point e per diversi fenotipi della sclerosi multipla. Sulla base dei risultati del presente studio, studi più ampi andrebbero incoraggiati ai fini di validare l'utilità della QSM per supportare la diagnosi e prognosticare il decorso della malattia. Studi multimodali sulla NAWM possono inoltre essere implementati per raggiungere una più completa caratterizzazione della NAWM in pazienti affetti da sclerosi multipla.

Contents

Glossary

ANTs: Advanced Normalization Tools

BBB: Blood Brain Barrier

BET: Brain Extraction Tool

CDMS: Clinically Defined Multiple Sclerosis

CIS: Clinically Isolated Syndrome

CNS: Central Nervous System

CSF: Cerebrospinal Fluid

DICOM: Digital Imaging and Communication in Medicine

DTI: Diffusion Tensor Imaging

EDSS: Expanded Disability Status Scale

FP: False Positive

FS: Functional Systems

GM: Grey Matter

GMF: Grey Matter Fraction

GRE: Gradient Echo

LCL: Lesion Change Labels

LGA: Lesion Growth Algorithm

LST: Lesion Segmentation Toolbox

MIP: Minimum Intensity Projection

MR: Magnetic Resonance

MS: Multiple Sclerosis

MTR: Magnetization Transfer Ratio

NAWM: Normal-appearing White Matter

NAWMF: Normal-appearing White Matter Fraction

P: Progressive

PACS: Picture Archiving and Communication System

PVE: Partial Volume Estimate

QSM: Quantitative Susceptibility Mapping

RIS: Radiologic Isolated Syndrome

ROI: Region Of Interest

RR: Relapsing-Remitting

SMV: Spherical Mean Value

SPM: Statistical Parametric Mapping

SPSS: Statistical Package for Social Science

STI: Susceptibility Tensor Imaging

SWI: Susceptibility Weighted Images

TE: Echo time

TPM: Tissue Probability Map

VOI: Volume Of Interest

WM: White Matter

WML: White Matter Lesions

List of figures

List of tables

Chapter 1

Introduction

This chapter is meant to provide an overview of the multiple sclerosis disease, its diagnosis and its features. It also gives a description of the tissues intrinsic characteristic known as *susceptibility* and an outline of the MRI multi-echo gradient-echo sequence to perform quantitative mapping of susceptibility.

The purpose of the thesis is briefly described in the last paragraph.

1.1 Multiple sclerosis

Multiple sclerosis is an autoimmune inflammatory chronic disease of the central nervous system (brain, optic nerves and spinal cord) characterized by the loss of motor and sensory function.

This disease has been recognised as one of the most common causes of neurological disabilities in young adults, with an estimated worldwide number of people suffering from this disease of more than two million[1]. The incidence of MS is actually increasing all over the world, together with the socioeconomic impact of the disease[2].

Clinically, many MS patients experience recurrent episodes of neurological impairment called *relapses*, but in most cases (60-80%) the course of the disease becomes chronic and progressive with time, leading to cumulative motor disability and cognitive deficits[1]. Indeed, this disease is traditionally considered a two-stage disease, the first one being an early inflammation responsible for relapsing-remitting (RR) disease, and the second one being a delayed neurodegeneration causing non-relapsing progressive (P) disease[3].

A more specific classification of MS phenotypes comprises also the first onset of potential MS known as *Clinically Isolated Syndrome* (CIS), which is the first clinical central nervous system demyelinating event, lasting more than 24h and consistent with MS but isolated in time and/or isolated in space, and further divides the progressive phase in *primary progressive MS* and *secondary progressive MS*.

Histologically, perivenular inflammatory lesions are evident in the earlier phases of the disease, resulting in what is considered to be the pathological hallmark of MS: demyelinating plaques[1][4][15]. Inflammation leads to damage of oligodendrocytes and demyelination, disrupting the relay of neuronal signals in the affected regions. As the disease progresses, white matter (WM) chronic active lesions increase in number, while remyelinating lesions decrease.

The most widely accepted theory is that this inflammatory process is caused by an autoimmune cascade, involving T-cells which target myelin self-antigens[5][6], but there is another hypothesis according to which myelin-specific T-cells may be naturally present in the human body and may expand to pathogenetic numbers due to the malfunction of immunoregulatory mechanisms[7].

Although it is commonly stated that the underlying cause of MS remains unknown, environmental, genetic, and infectious factors appear to be significant for the development of the disease[1]. In particular, the epidemiology of the disease indicates that low serum levels of vitamin D, smoking, childhood obesity and infection with the Epstein-Barr virus are likely to play a role in its development[2].

For what concerns the diagnosis of MS, the first criteria were based on clinical features suggestive of the central nervous system (CNS) demyelination. Then, with the advance of neuroradiological techniques such as magnetic resonance (MR) imaging, the need for clinical evidence was partially replaced by the radiological evidence: the establishment of McDonald criteria and their successive revisions gave rise to an approach based on the integration of clinical, laboratory and radiographic data[1]. Such criteria are based on the detection of the spatial and temporal dissemination of focal neurological deficits and on the exclusion of important differential diagnoses, together with analysis on the cerebrospinal fluid and data on MR imaging[8].

A standard baseline profile for serological investigations should include anti-nuclear antibody, vitamin B12 and thyroid function. Syphilis and immunodeficiency virus 1 serology are recommended. Depending on the clinical presentation human T-cell, lymphotropic virus 1 and 2 serology, anti-aquaporin-4 and anti-myelin oligodendrocyte glycoprotein antibody screening may be indicated[2].

As regards MR, it is a critical tool for both the diagnosis of early MS and the prediction of its future course, thanks to its high sensitivity: up to 70% of brain lesions develop without clinical evidence of relapse[9][10], and the new silent lesions, which may be defined as *radiological relapses*, appear up to 10 times more frequently than lesions associated with clinical relapses[11][12][13]. This is relevant if we consider that the number of lesions seems to be well correlated with the risk of conversion from the CIS to the *Clinically Defined Multiple Sclerosis* (CDMS)[1].

MRI parameters that are likely to predict such conversion include the presence of multifocal homogenous or ring-enhancing white matter lesions, T2-hyperintense lesions in the corpus callosum, T2-hyperintense lesions in the posterolateral compartment of the spinal cord and positivity for Barkhof criteria.

However, the exclusive usage of imaging for MS diagnosis is not feasible, since it may introduce diagnostic errors. This is due to a low specificity: hyperintense lesions in the

white matter of the CNS are detectable in a wide range of other pathological conditions or even in a small percentage of healthy individuals[1].

Current evidence suggests that disease modifying treatment should be started at early stages of the disease, since it is likely to have a significant impact on the evolution of the disease [14]. Therefore, the main priority is a reliable diagnosis as early as possible with the aim of a timely initiation of the treatment [8].

1.1.1 The Expanded Disability Status Scale (EDSS)

The most widely used method for quantifying disability in multiple sclerosis and monitoring changes in the level of disability over time is the *Expanded Disability Status Scale* (EDSS)[56].

The scale ranges from 0 (no disability) to 10 (death due to MS) with an increment of 0.5, that represents a higher level of disability.

The assessment of the disability through the EDSS is aided by a series of grades of impairment in each of the so-called *functional systems* (FS). Such systems represent networks of neurons in the brain which are responsible for particular symptoms, and they are:

- Pyramidal – muscle weakness or difficulty moving limbs
- Cerebellar – ataxia, loss of balance, coordination or tremor
- Brain stem – problems with speech, swallowing and nystagmus
- Sensory – numbness or loss of sensations
- Bowel and bladder
- Visual – problems with sight
- Cerebral or mental – problems with thinking and memory
- Other functions

Apart from the last one, which is dichotomous, all these groups are graded from 0 (normal) to 5 or 6 (maximal impairment).

Table 1.1 gives a brief explanation of each possible grade in the EDSS.

EDSS score	Description
0	Normal neurologic exam.
1,0	No disability, minimal signs in one FS.
1,5	No disability minimal signs in more than one FS
2,0	Minimal disability in one FS.
2,5	Minimal disability in two FS.
3,0	Moderate disability in one FS or mild disability in three or four FS, though fully ambulatory.
3,5	Fully ambulatory but moderate disability in one FS and more than minimal disability in several others.
4,0	Fully ambulatory without aid, self-sufficient, up and about some 12 hours a day despite relatively severe disability consisting of one FS grade 4 (others 0 or 1), or combinations of lesser grades exceeding limits of previous steps. Able to walk without aid or rest some 500 meters.
4,5	Fully ambulatory without aid, up and about much of the day, able to work a full day, may otherwise have some limitation of full activity or require minimal assistance; characterized by relatively severe disability, usually consisting of one FS grade 4 (others 0 or 1) or combinations of lesser grades exceeding limits of previous steps. Able to walk without aid or rest for some 300 meters.
5,0	Ambulatory without aid or rest for about 200 meters; disability severe enough to impair full daily activities (e.g. to work full day without special provisions). Usual FS equivalents are one grade 5 alone, others 0 or 1, or combinations of lesser grades usually exceeding specifications for step 4.0.
5,5	Ambulatory without aid or rest for about 100 meters; disability severe enough to preclude full daily activities. Usual FS equivalents are one grade 5 alone, others 0 or 1, or combinations of lesser grades usually exceeding those for step 4.0.
6,0	Intermittent or unilateral constant assistance (cane, crutch, or brace) required to walk about 100 meters with or without resting. Usual FS equivalents are combinations with more than two FS grade 3+.
6,5	Constant bilateral assistance (canes, crutches, or braces) required to walk about 20 meters without resting. Usual FS equivalents are combinations with more than two FS grade 3+.
7,0	Unable to walk beyond approximately 5m even with aid. Essentially restricted to wheelchair; though wheels self in standard wheelchair and transfers alone. Up and about in wheelchair some 12 hours a day. Usual FS equivalents are combinations with more than one FS grade 4+; very rarely, pyramidal grade 5 alone.

7,5	Unable to take more than a few steps; restricted to wheelchair; may need aid in transfer; wheels self but cannot carry on in standard wheelchair a full day; may require motorized wheelchair. Usual FS equivalents are combinations with more than one FS grade 4+.
8,0	Essentially restricted to bed or chair or perambulated in wheelchair, but may be out of bed itself much of the day; retains many self-care functions; generally has effective use of arms. Usual FS equivalents are combinations, generally grade 4+ in several systems.
8,5	Essentially restricted to bed much of the day; has some effective use of arm(s); retains some self-care functions. Usual FS equivalents are combinations, generally 4+ in several systems.
9,0	Helpless bed patient; can communicate and eat. Usual FS equivalents are combinations, mostly grade 4+.
9,5	Totally helpless bed patient; unable to communicate effectively or eat/swallow. Usual FS equivalents are combinations, almost all grade 4+.
10	Death due to MS.

Table 1.1: Expanded Disability Status Scale (EDSS)

1.1.2 White matter and grey matter atrophy in multiple sclerosis

Brain volume loss occurs naturally in healthy people and it is regionally variable, but pathologic changes well beyond what is seen in controls have been observed in many studies in patients with MS of different phenotypes[50]. Even though multiple sclerosis has been always considered a WM inflammatory disease, scientific evidence suggests that a grey matter involvement is implicated as well: grey matter atrophy develops faster than white matter atrophy and predominates in the initial stages of the disease, even without clinical symptoms[49] and independently from the amount of white matter lesions and from changes in their volume[50].

Losses in brain volume are not uniformly widespread. For what concerns the grey matter, they are mostly caused by tissue damage in particular regions[50] and possible regional volume loss patterns have been identified for different MS phenotypes. For instance, the first regions to become atrophic in patients with CIS or with RR MS are the posterior cingulate cortex and praecuneus, followed by the middle cingulate cortex, brainstem and thalamus. A similar sequence of atrophy has been detected in primary progressive multiple sclerosis, with the involvement of the thalamus, cuneus, praecuneus, and pallidum, followed by the brainstem and posterior cingulate cortex[51].

Brain atrophy has been shown to be correlated with physical impairment, leading to a worsening and a progression of disability[52]. In particular, a study[53] evaluated whether physical disability during follow-up was related either to grey matter or to white matter atrophy. This analysis stated that atrophy of grey matter was related to an increase in EDSS and a worsening in the functional assessment of the patients in a higher proportion than in the atrophy of white matter.

Not only does brain atrophy have an impact on physical disability of MS patients, but it also affects the cognitive field from a pre-morbid stage of disease known as *Radiologic Isolated Syndrome* (RIS). Indeed, a study reported that 27.6% of these patients had signs of cognitive deterioration and that cortical brain volume reduction related to a worse performance in cognitive tests[54]. Moreover, in patients with RR MS, regional brain atrophy has been found to be related to specific functional involvement. As an example, atrophy of the *corpus callosum* (CC) has been related to a worsening both in verbal fluency and attention tests, while atrophy of the anterior segment of the CC has been related to fatigue and its degree of severity[55].

1.1.3 Normal-appearing white matter (NAWM) abnormalities in multiple sclerosis

As previously described, WM lesions are a pathological landmark of MS disease and a very sensitive point of reference for the diagnosis of MS and other neurodegenerative diseases. However, scientific literature has proved that abnormalities in MS patients are present even in the regions of the white matter that appear radiologically normal, which are referred as *normal-appearing white matter* (NAWM).

Several suggestions of these abnormalities have been highlighted with disparate approaches, such as post-mortem brain examinations. For instance, immunohistochemical analysis which comprised immunostaining for myelin, axonal markers, activated microglia/macrophages, astrocytes plasma proteins and blood vessels suggested that the processes of axonal degeneration and microglial activation are actually present in the NAWM in proximity to WM lesions, and that the microglial activation is present far from WM lesions as well[63].

Another histological study also assessed the proliferation of astroglia within the NAWM of MS patients in relation to control groups, confirming the significantly higher microglia and astroglia proliferation compared to controls. Possibly, microglia support proinflammatory mechanism that leads to nervous tissue damage, while astrocytes seem to be more neuroprotective[64].

These histopathological observations highlight the importance of investigating the NAWM *in vivo*: different MR techniques are now able to yield different information, but they have some limits that restrict the disentangling of the heterogeneous processes that characterize MS pathology.

T1 relaxation time appears to be sensitive to subtle changes of the matter and has been demonstrated to be increased in MS NAWM, but it is not specific: changes of very different natures may induce a T1 elongation[62].

T2 relaxation times have also been measured in order to assess the myelin water fraction as a measure of tissue myelin content, and results seem to suggest that myelin integration is compromised in NAWM[62].

Another parameter that has been taken into consideration to assess NAWM abnormalities *in vivo* is the *magnetization transfer ratio* (MTR), which is extracted from *magnetization transfer* (MT) imaging. The decrease of this ratio is thought to reflect demyelination and/or axonal damage, and many studies have found that MTR was decreased in the NAWM of MS patients with respect to the NAWM of healthy controls.

Longitudinal MRI studies have also demonstrated a local MTR decrease several months prior to the appearance of a focal lesion, suggesting that some of the measured changes might be an early sign of developing lesion. On the other hand, changes are relatively small, MTR values are generally poorly comparable between scanners or centres, and the measure incorporates not only the effect of magnetization transfer, but also of longitudinal relaxation[62].

Finally, *diffusion tensor imaging* (DTI) studies have been performed in order to investigate the integrity of WM tracts by quantifying the overall degree to which water molecules could diffuse: results suggested that WM tract integrity is compromised in NAWM in MS[62].

In summary, the various techniques that have been utilized in order to assess NAWM abnormalities provide different information, but all the data seems to suggest that the NAWM is not as healthy as it radiologically seems. Moreover, neuropathological and imaging evidence suggests that pathological events could start from the earliest disease stages of multiple sclerosis, therefore these studies have brought about interest in the pathological meaning and clinical importance of the NAWM in MS.

1.2 Magnetic susceptibility in the biological matter

Magnetic susceptibility is an intrinsic property of the biological matter which refers to the magnetizability of a material when placed in an external magnetic field B_0[37]; it closely reflects tissue composition[38] and it is indicated with the symbol χ.
Mathematically, χ represents a proportionality constant between the material's macroscopic magnetization M and the local magnetic field B:

$$M = \chi\frac{B}{\mu_0} \approx \chi\frac{B_0}{\mu_0} \tag{1.1}$$

with μ_0 a physical constant representing the magnetic permeability of vacuum ($4\pi \times 10^{-7}$ H m^{-1}).

Susceptibility can be positive or negative, depending on whether magnetization aligns with the field (*paramagnetism*) or opposes to it (*diamagnetism*). Even though the theory of magnetism of different materials remains a very active field of research because of the complexity of fully understanding the collective behaviour of vast numbers of electrons in many different types of materials, a simple model of magnetism starting from noninteractive moments has been useful to understand the origin of paramagnetic and diamagnetic susceptibility. According to this model, magnetism is primarily contributed by the magnetic moments of electrons, with contributions from nuclear moments being negligible small[39].

In an atom or molecule, electrons are distributed into different energy levels and are characterized by a spin value $s = \pm \frac{1}{2}$. The orbital angular momentum is quantized as well, and this gives rise to a set of quantized magnetic moments:

$$\mu_s = -g_s\mu_B\frac{S}{\hbar} \approx \mu_B \tag{1.2}$$

$$\mu_L = -g_L\mu_B\frac{L}{\hbar} \tag{1.3}$$

where μ_S and μ_L are the magnetic moment of an electron resulting from its spin and angular momentum respectively, g is the Landé g-factor; S and L are the spin and orbital

angular momentum quantum number respectively, $\hbar$ is the reduced Planck constant and μ_B is the Bohr magneton. The probability of finding an electron with a given set of quantum numbers follows Boltzmann's distribution, which in turn gives an effective magnetic moment μ_{eff}. In the end,

$$\chi = \frac{C}{T} \sim \frac{\mu_{eff}^2}{T} \tag{1.4}$$

where C is the Curie temperature. As a rule of thumb, the more unpaired electrons there are, the larger the effective magnetic moment is, because paired electrons tend to cancel each other[39]. This is the case of *paramagnetism*, which applies to a very small fraction of biological molecules, especially those containing transition elements such as iron, copper and manganese which have unpaired valence electrons[37]. Molecules which develop such kind of magnetizability are called *open shell molecules*.

On the contrary, most of the biological molecules feature a total spin S equal to 0, since they generally have even numbers of electrons and all their spin-up electrons are paired with spin-down electrons[37]. This is the case of *closed shell molecules*, which have a very feeble negative magnetizability and are called *diamagnetic*. This phenomenon can be explained with the fact that, in addition to the aforementioned paramagnetism, the presence of an external field also causes the electrons to precess about the applied field, generating a secondary field that opposes the applied field. The precession of electrons is modelled as a circular current. According to a classic model of nonquantum mechanics known as *Langevin model*, the magnetic moment of this induced current is:

$$\mu = -\frac{Ne^2\mu_0 B}{4m_e}\rho^2 \tag{1.5}$$

where N is the number of electrons per unit volume, e is the electron charge, m_e is the electron mass, μ_0 is vacuum permeability and ρ^2 is the mean square distance of the electrons perpendicular to the field B direction[39]. Therefore, the diamagnetic susceptibility is:

$$\chi = -\frac{\mu_0 N e^2}{4 m_e} \rho^2 \qquad (1.6)$$

Figure 1.1 summarizes paramagnetic and diamagnetic susceptibility[39].
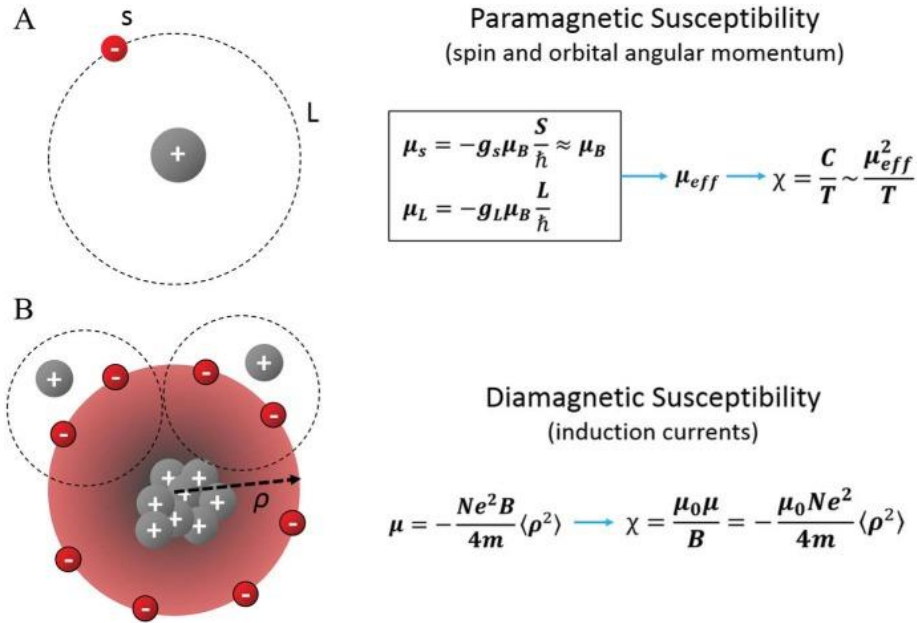
Figure 1.1: Paramagnetic and diamagnetic susceptibility

1.2.1 Susceptibility in multiple sclerosis

Due to the abundance of water, healthy human brain tissues are characterized by a rather weak diamagnetic susceptibility dominated by this molecule (χ = -9.95 ppm)[37]. Nonetheless, an imbalance of certain ions or the disruption of certain structures can cause an alteration in susceptibility, as it will be explained in the following paragraphs.

Another contribution to susceptibility is represented by blood, more specifically by oxygenation, which changes haemoglobin from being paramagnetic (deoxyhaemoglobin) to being diamagnetic (oxyhaemoglobin). However, haemoglobin does not play any significant role in affecting the susceptibility contrast between grey and white matter[46].

1.2.1.1 Iron contribution to susceptibility

Iron is the most abundant trace metal in the healthy human brain, with a concentration 20 to 30 times higher than all the other trace metals combined[16], increasing linearly with age for about 20 years, staying almost constant for the next 40 years and then increasing further with age[17].

Brain iron is stored in the tissue cells where neurochemical processes require iron, primarily in oligodendrocytes and myelin[18]. The highest iron concentrations are found in the nuclei of the deep grey matter in the midbrain, including globus pallidus, red nucleus, substantia nigra and putamen, where the synthesis of neurotransmitters such as dopamine and glutamate seems to require electron facilitation by iron[21]. A significant amount of iron is also found in cortical grey regions including the motor, occipital, sensory and prefrontal cortex[21].

In the white matter, iron level is more homogenous compared to the grey matter, with a higher concentration in the frontal lobe and a lower concentration in the occipital lobe compared to adjacent cortical GM, therefore featuring a gradient in iron concentration[22][23]. In particular, oligodendrocytes contain large amounts of iron because of their large metabolic activity, including the synthesis of myelin[15].

Most of the brain iron is present as the inactive form of ferric iron (Fe^{3+}) stored in the spherical shell of protein ferritin, while a slight amount corresponding to less than 5% is present in the active form of ferrous iron (Fe^{2+}). The former can be rapidly converted into the latter by reductants and chelators[18], but also the opposite conversion is possible thanks to the H-subunit of ferritin which is able to oxidize ferrous iron into ferric iron and to store it in ferritin[19].

The overall iron level is maintained by a precise homeostasis mechanism that is critical for healthy brain function and that involves iron-regulating proteins for ferritin, iron transporters and transporters receptors[20].
The disruption of such homeostasis is associated to neurological diseases and neurodegeneration[15][21], since iron acts as a cofactor for various enzymatic reactions, specifically the synthesis and maintenance of myelin[36]. Indeed, excessive brain iron levels are invariably associated with neurodegenerative diseases such as Alzheimer's disease, amyotrophic lateral sclerosis, Parkinson's disease[15] and MS.

Iron is considered to play a key role in the development and progression of MS, since the accumulation of this metal in myeloid cells after the BBB may contribute to chronic inflammation, oxidative stress and eventually neurodegeneration.

Increased iron deposition has been observed in the nuclei of the deep grey matter, primarily in the putamen[29][30]. Furthermore, iron accumulation in the basal ganglia during aging is accelerated in neurodegenerative diseases[31].

It is also documented that iron is retained by microglia and macrophages during inflammation[24][36]. More precisely, the iron uptake relies on the spectrum of phenotypes that can be assumed by these cells, which may include a band of pro-inflammatory activation known as *M1* or a band of anti-inflammatory *M2* activation. As a matter of fact, M1 polarization is associated with high intracellular iron content, while M2 is associated with enhanced iron release and low intracellular iron[25][26].
Moreover, it has been showed that the iron uptake itself promotes a pro-inflammatory state in macrophages, thus preventing the physiological switch from M1 to M2 activation associated with wound healing[36]. One proposed mechanism is that high intracellular iron leads to the activation of nuclear factor-kappa B (NF-κB), a master regulator of the innate and adaptive immune system[27][28], leading to expression of NF-κB target genes including pro-inflammatory cytokines[36].

Regarding WM lesions, a remarkable finding is that iron is absent from early active lesions, since in this phase macrophages contain fragments of myelin and are M2 polarized[32]. However, over the course of time, chronic active lesions show no or minimal active demyelination but contain iron-rich microglia, predominantly at the lesions rim[33]. The presence of iron in these microglia cells may be due to the release into the extracellular space of the metal upon the destruction of oligodendrocytes and myelin[34], and it is likely to propagate chronic and pro-inflammatory activation that may contribute to neurodegeneration and disease progression[15]. In this stage, microglia and macrophages show an M1 activation[36]. Eventually, if the lesions become chronic silent, the level of iron decreases as the level of inflammatory cells decreases[35][36].
Figure 2.1 summarizes the characteristics of lesions over the course of time[36].

Because of its paramagnetism, the level of iron in the tissues influences their susceptibility. For instance, susceptibility increases in chronic active lesions because of the accumulation of iron inside the microglia, but changes in susceptibility are also likely to happen in the NAWM because of the aforementioned abnormalities, namely inflammation and consequent microglia proliferation.

Acute lesions

Myelin⁺, iron⁻ macrophages

Open BBB
Gadolinium enhancement
Active demyelination
M2 marker expression by macrophages

Chronic active lesions

Myelin⁻, iron⁺ microglia

Closed BBB
High tissue susceptibility (QSM)
No/slow demyelination
M1 marker expression

Chronic silent lesions

Closed BBB
No enhancement/low susceptibility
No demyelination
No inflammatory cells

Figure 1.2: MS lesions characteristics over the course of time

1.2.1.2 Myelin contribution to susceptibility

Besides iron, another major contribution to susceptibility is myelin, which ensheaths most of the longer axons in the brain in order to accelerate nerve conduction. Myelin is formed by oligodendrocytes and consists of multiple phospholipid bilayers (5-20 or more) which contain lipids, proteins and little water (<20%). The diamagnetism of phospholipids that constitute the myelin sheath has been considered to be the primary cause of WM susceptibility, which is the most diamagnetic tissue in healthy brains[37].

Myelin is essential for the proper functioning of the nervous system: loss of the myelin sheath is the hallmark of a number of neurodegenerative autoimmune diseases, including MS[46]. Because of the diamagnetism of phospholipids, this loss is also the cause of an increased susceptibility in the tissues where the destruction of the sheath has happened.

1.3 Gradient echo (GRE) multi-echo sequences

Several *in vivo* MR techniques which are able to assess NAWM abnormalities have been presented in 1.1.3, each one with its own restraints that make the understanding of these heterogeneous anomalies still challenging.

In this scenario, susceptibility changes within tissues seem to be a promising indicator of the underlying pathologic signs, since in the magnetic field of an MRI scanner susceptibility differences cause variations in the local magnetic field strength[38] and, consequently, they constitute an opportunity to sense the microscopic distribution of iron and myelin.

The MRI technique that is commonly used to evaluate susceptibility changes is the gradient echo multi-echo sequence, which implies the initial application of an external dephasing gradient field across the tissue, slightly altering the resonance frequencies across the tissue and causing a calibrated change in local magnetic field, and the subsequent reversal of the process with the application of a rephasing gradient with the same strength but opposite polarity. Field inhomogeneities are the cause of a non-complete rephase by the gradient reversal, hence the amplitude of the gradient echo decays with a time constant indicated by T_2^{**}.

This sequence is exploited both in *susceptibility weighted imaging* (SWI), which is able to provide contrast-enhanced images by using the susceptibility differences between tissues[46], and in *Quantitative Susceptibility Mapping* (QSM), which is the object of this thesis. Although these techniques share the usage of GRE sequences, SWI is actually a non-linear filter which is applied by the MR scanner to give a susceptibility weighting to the MR images already during their acquisition, whereas QSM is a post-processing of MR images that is done after their acquisition with specific software.

Tissue susceptibility can affect both amplitude and frequency of gradient echo signals because the resonance frequency f of water ^{1}H protons depends on the field B that they sense:

$$f = \frac{\gamma}{2\pi} B \qquad\qquad (1.7)$$

where γ is the gyromagnetic ratio of ^{1}H protons and B is a combination of both the applied static field B_0 of the scanner and the field shift B created by the magnetization M of the object which, according to (1.1), depends on susceptibility. Even though variations in χ are often small (in the order of 0.1 ppm), they actually lead to easily detectable frequency shift[37] and result in phase differences in gradient-echo MR images[38].

The amplitude of the signal is affected as well, because field variations within voxels result in a distribution of resonance frequencies and consequently in decoherence and loss of the signal with a single-exponential decay rate indicated with R_2^* ($R_2^* = 1/T_2^*$)[37].

Susceptibility weighted imaging (SWI) is sensitive to both paramagnetic and diamagnetic substances since they generate different phase shifts in MRI data, and it is created by combining both magnitude and phase in the gradient echo data (GRE)[46].

Although T_2^*-weighted magnitude image already provide some susceptibility contrast, SWI is able to enhance the contrast between tissues which feature different susceptibility. More specifically, SWI combines a T_2^*-weighted magnitude image with a filtered phase image acquired with the gradient echo sequence in a multiplicative relationship[46].

The usage of a filtered phase image is necessary since the raw GRE phase image is affected by an artifact known as *wrapping*, which occurs because sine and cosine functions are periodic with a period of 2π, hence any angle outside the range between $-\pi$ and π will be folded back.

In addition, the phase value within the brain is also influenced by the phase of the receiver coils, the long-range magnetic dipole field generated by the human body itself, and the large susceptibility difference between tissue and air. All the sources which contribute to phase outside the region of interest give rise to the so-called *background phase.* The presence of large background phase not only disguises local tissue contrast, but also worsens phase wrapping.

Figure 1.3 reports a visual representation of phase wrapping[46].
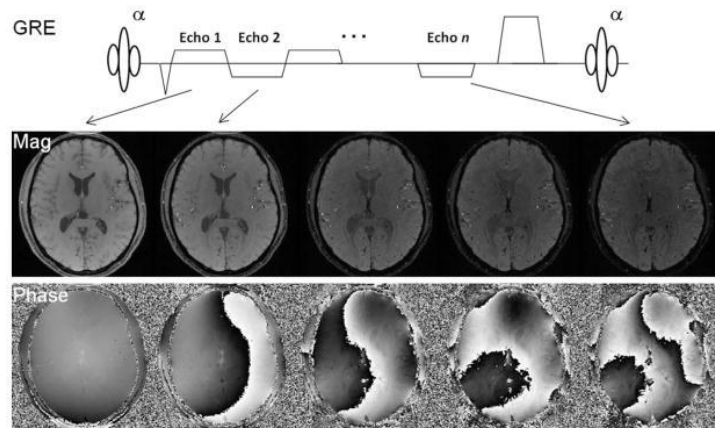
Figure 1.3: Phase wrapping artifact

A common approach in SWI is to perform a phase unwrapping procedure followed by a high pass filtering operation with the assumption that the background phase is smooth and only contains low spatial frequencies.

After the filtering, what is obtained is a phase mask with an amplitude in the range from 0 to 1, which is multiplied several times with the original GRE magnitude image in order to create the aforementioned contrast between tissues with different susceptibilities. The number of phase mask multiplications may vary as a function of the phase difference and the contrast-to-noise ratio.

In order to further enhance the contrast, another last step that could be done is the *Minimum Intensity Projection* (MIP).

Figure 1.4 summarizes all the steps which are necessary in order to obtain a SWI image[46].
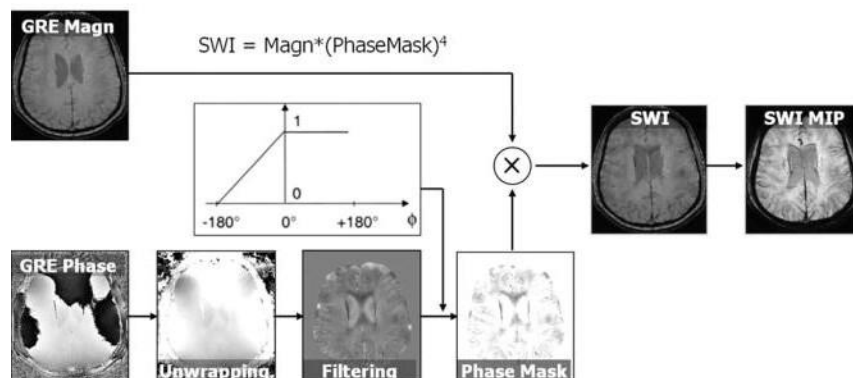
Figure 1.4: SWI pipeline

The biggest limitation of SWI is obviously the inability to provide quantitative measures of magnetic susceptibility: in order to overcome such constraint, Quantitative Susceptibility Mapping (QSM) is needed[39].

1.3.1 Quantitative Susceptibility Mapping (QSM)

Quantitative Susceptibility Mapping (QSM) is an MRI technique for quantifying the spatial distribution of magnetic susceptibility within biological tissues[39].
This technique is based on the assumption that phase shifts in phase images of gradient echoes (GREs) are primarily due to susceptibility-induced field inhomogeneity. However, the phase measured in GRE acquisitions strongly depends on imaging parameters and phase values are nonlocal, meaning that the phase values measured in a voxel depend not only on local tissue properties, but also on the surrounding magnetic susceptibility distribution. Nevertheless, by treating the susceptibility-induced magnetization as a magnetic dipole, the field perturbation caused by a known distribution of isotropic susceptibility can be obtained by convolving the susceptibility distribution with a unit dipole kernel[39].
In other words, the magnetization of an imaging voxel is treated as a magnetic dipole and each dipole produces a magnetic dipole that extends in space beyond the voxel itself. Consequently, the magnetic field at any given voxel is a superimposition of all dipole fields generated by the surrounding voxels, but the superimposition of magnetic field is linear and the field of a unit dipole is shift invariant, meaning that it does not change from one voxel to another. Hence, the relationship between the spatial distribution of susceptibility and the spatial distribution of frequency is governed by a convolution and the impulse response is the unit dipole field[46].

Convolution in the image domain can be performed in an easy and efficient way as a pointwise multiplication in the k-space, such that:

$$\Delta B_z(k) = B_0(\frac{1}{3} - \frac{k_z^2}{|k^2|})\chi(k) \tag{1.8}$$

where k is the k-space vector and k_z its z-component, B_0 is the applied magnetic field, taken to be in the z-direction, $\Delta B_z(k)$ is the Fourier transform of the z-component of the

magnetic field perturbation and χ(k) is the Fourier transform of the magnetic susceptibility distribution[39].

The inversion of this equation solves the problem of nonlocality of phase and allows to obtain the QSM. On the other hand, the measurement of ΔB_z and the ill-posed nature of the inversion itself constitute two challenges for the QSM technique.

ΔB_z may be calculated from the GRE signal phase by scaling the measured phase by the gyromagnetic ratio and echo time to generate a field map. However, the phase considered must be the one caused by susceptibility and not by other effects such as receiver-coil (B_1 field), flow-induced phases and chemical shifts: once the susceptibility-induced phase is isolated, data must be processed in order to remove phase wraps and the contribution of background fields generated by sources outside of the volume of interest (VOI).

In particular, the magnitude images acquired with the GRE sequence are used to create a mask of the brain that provides the volume of interest (VOI), while the phase images are first unwrapped and then filtered by a background phase filtering in the masked region. The filtered phase is then divided by the TE to obtain a map of frequency variation with respect to the reference frequency of the scanner.

The local field perturbation is then given by:

$$\Delta B_z(k) \;=\; \frac{\Delta \omega}{\gamma} \tag{1.9}$$

where $\Delta \omega$ is the local frequency perturbation and γ is the gyromagnetic ratio[39].

Building a susceptibility map from the local tissue field map is more complex: the field map must be deconvolved with the unite dipole kernel, corresponding to a pointwise division in the k-space. However, this deconvolution is an ill-posed problem because of zeros in the k-space dipole kernel on two conical surfaces at approximately 54.7° with respect to the main magnetic field, in which the inverse kernel is undefined[39]. Consequently, susceptibility cannot be accurately determined in regions near the conical surface[46].

Furthermore, noise is highly amplified in regions where the kernel is very small and the inverse kernel is very large, and this makes the inversion of the forward calculation

impossible. For these reasons, QSM is achieved by conditioning of the ill-posed inverse calculation to measure the susceptibility distribution while excluding or minimizing noise and artifacts. Iterative fitting algorithms to create susceptibility maps by estimating the susceptibility distribution as a solution of a minimization problem have been proposed as well, in addition to the conditioning of the direct inverse calculation[39].

The result of QSM is a quantitative susceptibility map where, as a convention, brighter intensities represent paramagnetic susceptibility, whereas dark intensities represent diamagnetic susceptibility[46].

Figure 1.5 reports the whole QSM pipeline[39].
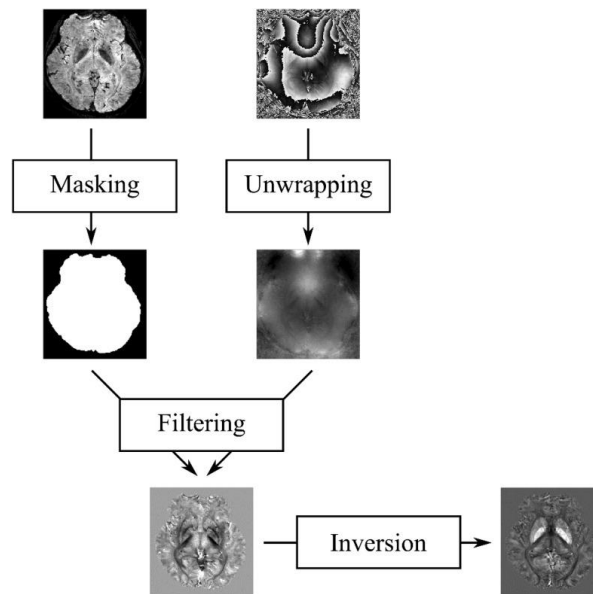
Figure 1.5: QSM pipeline

QSM's accuracy is limited by its inherent assumption that that the susceptibility is isotropic in nature, while in reality some molecules such as lipids in myelin, collagen and α-helix polypeptide have been shown to have anisotropic susceptibility which can be described by a susceptibility tensor. This is the basis of a novel application called *susceptibility tensor imaging* (STI) in which such tensor is used to create an orientation-dependent magnetization when exposed to a magnetic field[39].

Another limitation of QSM is that the susceptibility values measured by QSM are basically determined by the molecular composition within an imaging voxel. Each voxel contains a wide range of molecules of different kinds, all situated within a complex cellular

environment. Due to the finite resolution of MRI, susceptibility determined by QSM is just a sampled approximation of the true susceptibility distribution[39]. Nevertheless, in several experiments, QSM has been shown to find the magnetic susceptibility distribution underlying the measured MRI signal with a good accuracy[40][41].

1.3.1.1 Clinical applications of QSM

Biological cells contain a myriad of molecules and ions, each one characterized by its own magnetic susceptibility. Hence, by studying the pathological state and concentration of physiologically significant molecules in diseased tissues, QSM is being evaluated in a growing number of clinical applications[39].

MRI measurements such as lesion number or total lesion volume have been shown not to predict multiple sclerosis progression[42]. On the contrary, QSM has become increasingly prominent in order to detect tissue changes that occur in MS: for instance, scientific literature asserts an increased susceptibility in the deep grey matter in patients with clinically definite MS or a clinically isolated syndrome that suggests MS[43][44][45]. However, most of the studies have been concentrated on the quantification of iron levels and susceptibility inside the deep grey matter[39], while a thorough study of susceptibility in the other parts of the brain is still under research. Given the presence of abnormalities in the NAWM in MS, assessing this tissue with QSM might constitute a non-invasive approach for a better understanding of the physiopathology of this disease.

1.4 Aim of the study

The aim of the study is to characterize the normal-appearing WM and the WM lesions in MS time course and phenotypes by QSM, and to correlate quantitative QSM measures to clinical measures.

Two pipelines have been developed in order to obtain the mean value of susceptibility inside the NAWM and the lesions: the first one regards two different groups of patients (G0 and G1) at two different time points, which have been defined based on the time elapsed between the MRI data acquisition and the diagnosis of multiple sclerosis; the second one regards a longitudinal group of patients whose MRI data was available at both time points (T0 and T1). In this case, the pipeline assesses not only the mean value of susceptibility in the NAWM and the lesions, but also in the lesion areas that have increased/not changed/decreased between the two time points.

Statistical analysis has been carried out as well, in order to test differences in the neuroimaging measurements between groups and time points and to establish a relationship among the most significant neuroimaging measurements and the clinical variables.

Chapter 2
Methods

This chapter provides a description of the magnetic resonance data that has been used for this study and an explanation of every passage of the image processing pipelines that have been implemented in order to quantify susceptibility inside the NAWM and the lesions.

Finally, an overview of the statistical analysis that has been carried for both the pipelines out is provided.

2.1 Participants recruitment

Fifty-nine patients with a new diagnosis of multiple sclerosis (MS) according to the 2017 revised McDonald criteria[8] were recruited at the Neurodegenerative Diseases Unit of *Fondazione IRCCS Ca' Granda Ospedale Maggiore Policlinico* (Milano).

All patients underwent clinical assessment, lumbar puncture and brain MRI. For each recruited patient, the Expanded Disability Status Scale (EDSS) score was assessed in two time points, the first one being at less than 6 months from the diagnosis of MS (T0) and the second one being after more than 6 months from their diagnosis of MS (T1).

Thirty-eight patients underwent MR at T0, and thirty-four patients underwent MR at T1. According to the time point of the MRI acquisitions, patients were split into two different groups (see table 2.1):

- **G0**: patients whose magnetic resonance images were acquired in a time interval of less than 6 months from their diagnosis of multiple sclerosis
- **G1**: patients whose magnetic resonance images were acquired after more than 6 months from their diagnosis of multiple sclerosis

Within both G0 and G1 groups, patients were also subdivided according to their specific MS phenotype:

- **RR:** Relapsing-Remitting phenotype
- **P:** Progressive phenotype (considering both secondary progressive and primary progressive)

The main demographic and clinical characteristics of G0 and G1 patients are summarized in tables 2.1 and 2.2.

Group	Age		Male/Female
	Median	**Interquartile range**	
G0	32,64	26,08 - 43,87	13/25
G1	38,50	30,41 - 52,50	21/13

Table 2.1: Demographic data of patients for each group

Group	Disease duration (months)		EDSS		RR/P
	Median	Interquartile range	Median	Interquartile range	
G0	0,00	0,00 - 1,25	2,00	1,00 - 2,50	32/6
G1	15,07	9,08 - 22,03	1,75	1,00 - 2,12	25/9

Table 2.2: Clinical data of patients for each group

2.1.1 Longitudinal study group

Thirteen of the patients were recruited for the longitudinal study and, after the MRI data acquisition within 6 months their diagnosis of multiple sclerosis (T0), repeated the MRI scan at 1-year follow-up (T1).

When mentioning this longitudinal study group, the two time points in which the magnetic resonance data was acquired will be referred to:

- **T0**: time point in which the first magnetic resonance scan was performed, distant less than 6 months from the diagnosis of multiple sclerosis

- **T1:** time point in which the second magnetic resonance scan was performed, after more than 6 months from the diagnosis of multiple sclerosis

Table 2.3 summarizes the numeric data of all the study groups.

Number of G0 MRI data	Number of G1 MRI data	Number of longitudinal study (T0-T1) patients
38	34	13

Table 2.3: Numeric data of the study group

The demographic and clinical characteristics of the longitudinal study subgroup are reported in tables 2.4 and 2.5.

Time point	Age		Male/Female
	Median	Interquartile range	
T0	42,83	30,73 - 53,16	5/8

Table 2.4: Demographic data of the longitudinal study group

Time point	Disease duration (months)		EDSS	
	Median	Interquartile range	Median	Interquartile range
T0	0,00	-0,02 - 2,32	2,00	2,00 - 3,25
T1	9,17	5,70 - 13,48	2,00	0,50 - 2.50

Table 2.5: Clinical data of the longitudinal study group

2.2 Images acquisition

Whole brain images were acquired in a 3T Philips Achieva d-Stream scanner. Three sequences in particular were used, with the following parameters:

- 3D T1-weighted images: Repetition time = 7,58ms; Echo time = 3,54ms; Pixel spacing = 1,00mm; Slice thickness = 1,00mm; Spacing between slices = 1,00mm; Flip angle = 8°; Rows = 256; Columns= 256.

- 3D FLAIR images: Repetition time = 4800ms; Echo time = 320,13ms; Pixel spacing = 0,52mm; Slice thickness = 1,00mm; Spacing between slices = 0,50mm; Flip angle = 90°; Rows = 480; Columns= 480.

- Spoiled gradient-echo (GRE) multi-echo sequence: Repetition time = 51,00ms; Number of echoes = 6; Echo time = 9,80ms-17,00ms-23,00ms-30,00ms-37,00ms-44,00ms; Pixel spacing = 0,45mm; Slice thickness = 2,00mm; Spacing between slices = 1,0mm; Flip angle = 20°; Rows = 512; Columns = 512.

MR images were clinically evaluated and processed at Neuroradiology Unit, *Fondazione IRCCS Ca' Granda Ospedale Maggiore Policlinico*.

2.3 Image processing pipeline

The pipelines implemented to process the images are described in figures 2.1 and 2.2; each step will be discussed in the following paragraphs.

The first pipeline has been applied both to G0 and to G1 patients in order to obtain a ROI-based extraction of the mean value of susceptibility inside the NAWM and the lesions.

Such pipeline is represented in figure 2.1.
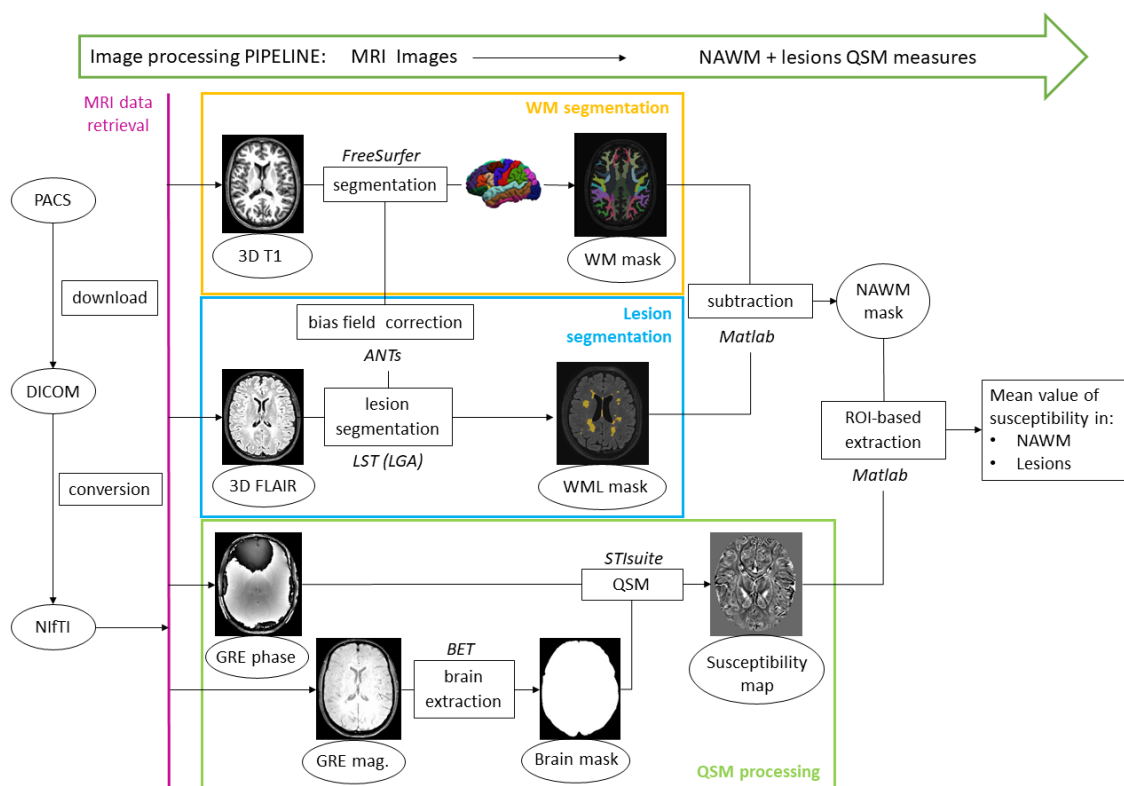
Figure 2.1: Pipeline 1, applied to G0 and G1 patients

The second pipeline, on the other hand, has been applied only on the longitudinal study group in order to obtain the mean value of susceptibility not only inside the NAWM and the lesions, but also inside the lesion areas that have been decreased/not changed/decreased between the two time points.

Figure 2.2 graphically represents such pipeline.
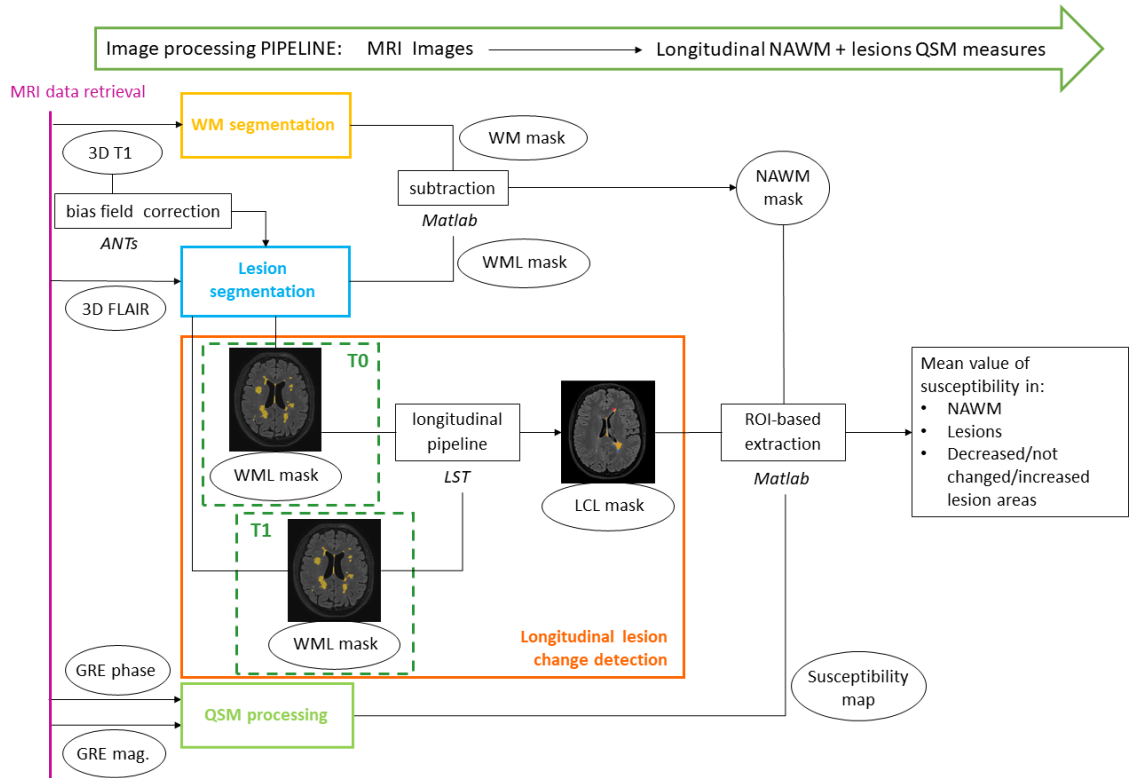
Figure 2.2: Pipeline 2, applied only for the longitudinal study group

2.3.1 Pre-processing

The image processing pipelines take as input the 3D T1-weighted images, the 3D FLAIR images and the spoiled GRE multi-echo images.

These three sequences were stored in *Digital Imaging and Communication in Medicine* (DICOM) format and were retrieved from the hospital's *Picture Archiving and Communication System* (PACS). However, due to the excessive dimension of the DICOM format, NIfTI format is generally preferred in neuroimaging processing. Hence, images were converted to such format by using *dcm2niix* function in the software *MRIcroGL*.

Figure 2.3 and figure 2.4 show the images that were employed in the processing pipeline.
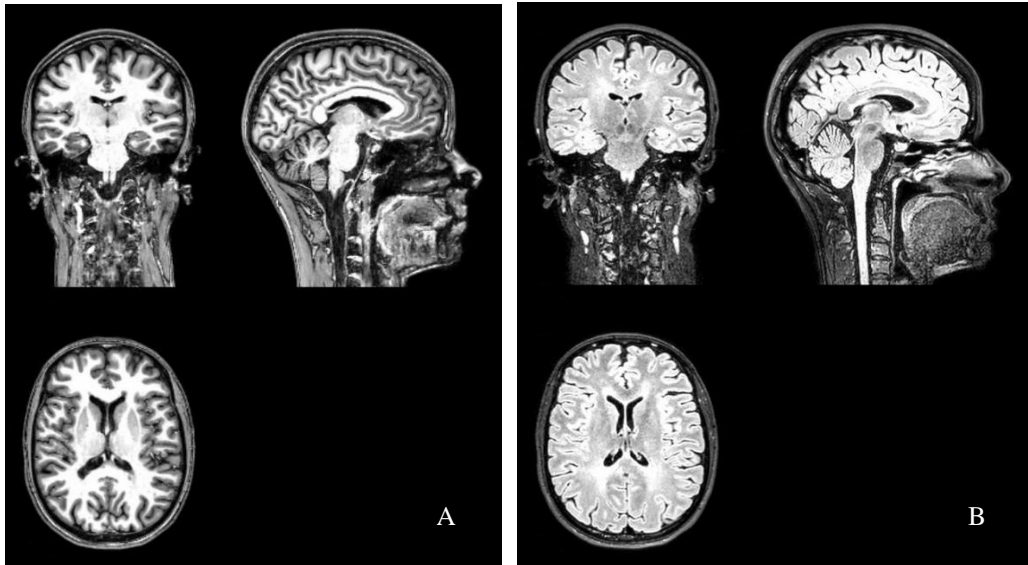
Figure 2.3: Coronal, sagittal, axial 3D T1 (A) and FLAIR (B)
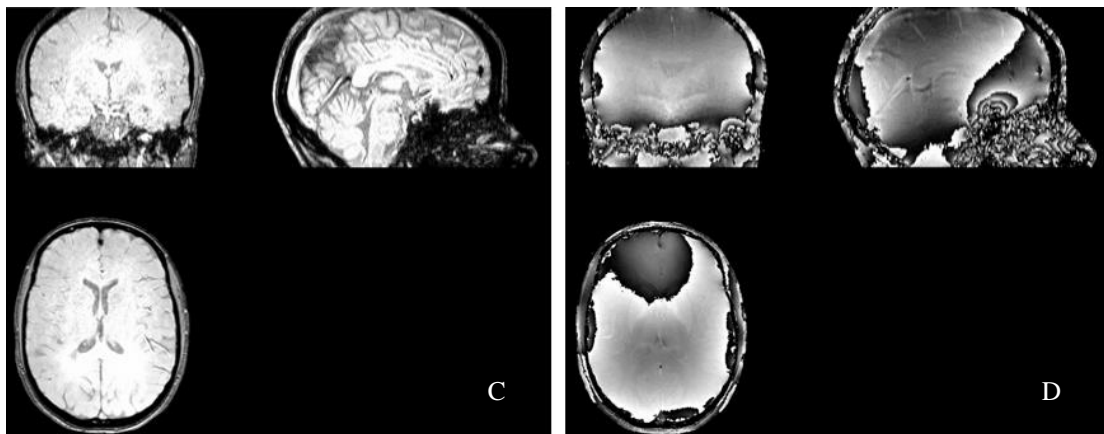
Figure 2.4: Coronal, sagittal, axial magnitude (C) and phase (D) of the first echo of the GRE sequence

2.3.2 Subcortical WM segmentation

The open source software *FreeSurfer* was utilized to segment the subcortical white matter, with an automated method for regional parcellation of the subcortical WM that uses curvature landmarks and GM/WM surface boundary information[61]. This requires as input the 3D T1 images that need to be segmented and returns as output a labelled atlas of the brain in which every brain structure for each hemisphere is tagged with a specific index. Since this thesis is focused on the study of the NAWM, all the structures corresponding to the WM were unified in order to create a single WM mask.

Examples in which such masks are superimposed to the corresponding 3D T1 image are reported in figures 2.5 and 2.6.
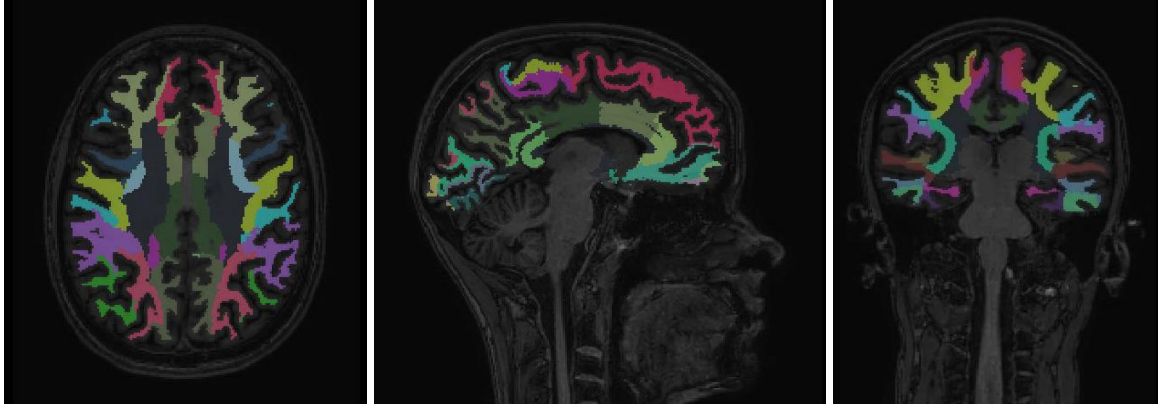
Figure 2.5: Segmented subcortical WM superimposed on a 3D T1 image
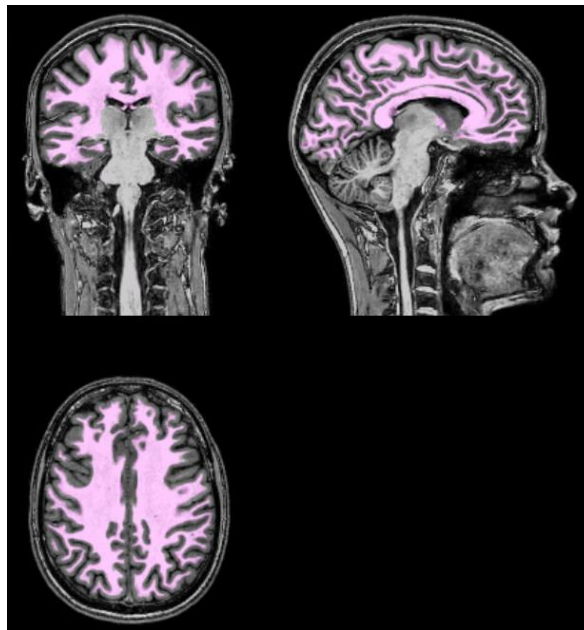
Figure 2.6: Whole segmented subcortical WM superimposed on a 3D T1 image

2.3.3 Lesion segmentation

2.3.3.1 Automatic lesion segmentation

MS lesions were segmented by using the *Lesion Growth Algorithm* (LGA)[47] as implemented in the LST toolbox version 3.0.0 for MATLAB's *Statistical Parametric Mapping* 12 (SPM12).

The algorithm operates in the space of original T1-weighted image, and it first segments this image into the three main tissue classes (CSF, GM and WM). The native T1 image is also used to generate a partial volume estimate label (PVE-label).

The tissue class containing the lesions is the WM, therefore the tissue probability map of white matter (TPM_{WM}) is warped into native space.

Then, the FLAIR image undergoes correction for a low-frequency intensity non-uniformity known as *bias field* and coregistration to the T1-weighted image. FLAIR intensity distributions are calculated for each of the three tissues classes in order to detect FLAIR-hyperintense outliers, which are further weighted according to their spatial probability of being WM. The results of these operations are lesion belief maps B_{WM}, B_{CSF}, B_{GM} which are summed up to B.

According to the pre-chosen initial threshold κ, the binary version of the GM lesion belief map is used as initial lesion map (L_{init}). Finally, the lesion growth model expands the L_{init} map toward the lesion belief map B, along voxels that appear hyperintense in the FLAIR image: neighbouring voxels are analysed and assigned to lesions under certain conditions. This is done iteratively until no further voxels are assigned to lesions. Herein, the likelihood of belonging to WM or GM is weighed against the likelihood of belonging to lesions. The result is a lesion probability map, meaning that each voxel can assume a value in the range from 0 to 1 according to its probability of representing a lesion voxel.

The whole LGA pipeline is summarized in figure 2.7[47].

The optimal threshold κ was chosen by visual inspection, comparing the results obtained by setting disparate thresholds. Different results were assessed also as a function of possible additional pre-processing. The final decision, validated by an expert neuroradiologist, was to set the threshold at 0.08 and to perform a bias field correction also in the 3D T1 images given as input to the algorithm. Such correction was done by using the *N4BiasFieldCorrection* function of the open source tool *Advanced Normalization Tools* (ANTs).

LGA outputs comprise a bias field corrected version of the FLAIR image that is coregistered to the 3D T1 image called *rmFLAIR* and a *Matlab* file which contains all necessary components that are needed for a re-run of the algorithm, as well as the lesion probability map which is in the same space of the *rmFLAIR*.
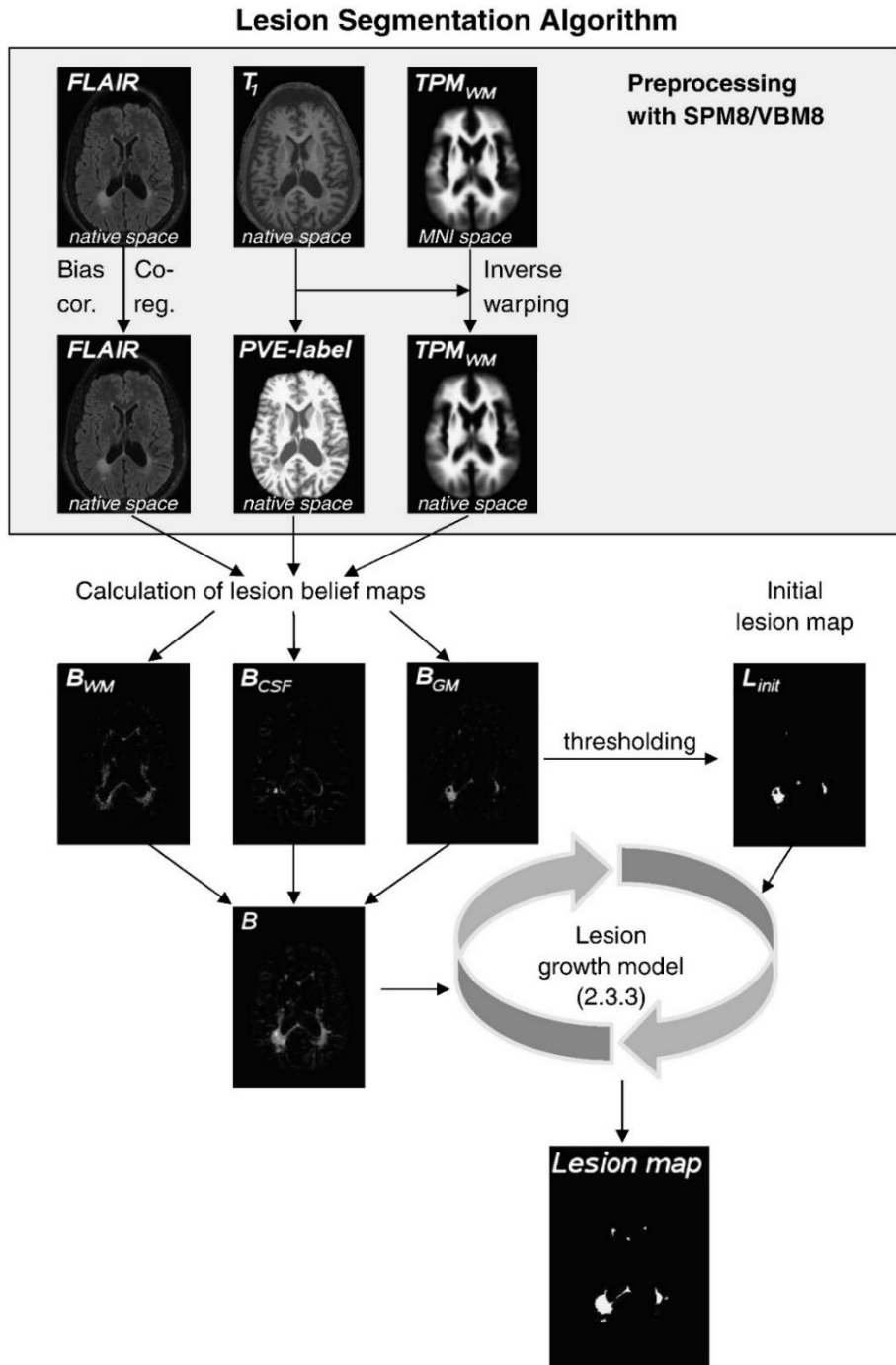
Figure 2.7: LGA pipeline

An example of the automatic segmentation of lesions performed by the LGA algorithm for SPM12 and superimposed to the corresponding *rmFLAIR* is shown in figure 2.8.
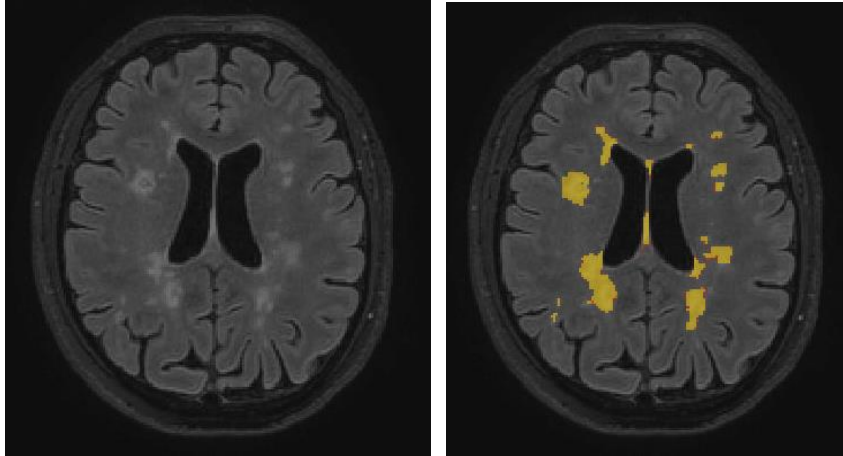
Figure 2.8: Example of the automatic segmentation performed by the LGA

2.3.3.2 White matter masking

The Lesion Segmentation Tool (LST) is a quite reliable method to segment MS lesions[47]. However, some false positives (FP) were detected by visual inspection in the GM, whereas the focus of the study was on WM lesions. For these reasons, the lesion maps were multiplied by the WM mask obtained with the software *FreeSurfer,* obtaining a WM lesions (WML) mask.

2.3.3.3 Manual refinement

The last passage regarding lesion segmentation was to manually refine the WML maps obtained by the two previous steps, in order to further increase the precision of such maps. This was done by expert neurologists.

2.3.4 NAWM segmentation

Both the WML mask and the *FreeSurfer* WM segmentation are in the same space, which is that of the 3D T1 images. Hence, in order to create a NAWM mask, it has been possible to subtract the WML mask from the WM mask using the software *Matlab*.
In this way, a mask comprising the whole WM except for WM lesions was obtained.
An example of NAWM mask is reported in figure 2.9.
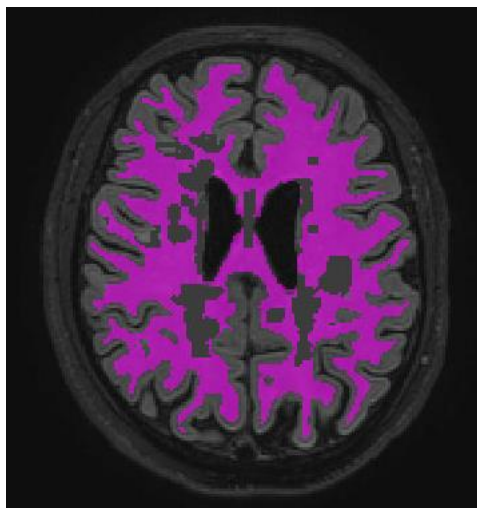
Figure 2.9: Example of NAWM mask

2.3.5 Longitudinal lesion change detection

The longitudinal lesion change detection was applied exclusively to the MR data of the longitudinal study group, since this subgroup comprises the patients whose magnetic resonance images were acquired at both T0 and T1 time points.

The Lesion Segmentation Tool (LST) provides the so-called *longitudinal pipeline*, which is able to perform a serial analysis of FLAIR-hyperintense WM lesions[48]. The input to this algorithm consists of the segmented lesions maps of the two different time points, together with the T1 and FLAIR images which were used to obtain them by the LGA.

Since the images of both time points have to be in alignment with each other in order to compare the segmented WML maps, the first step of the longitudinal pipeline is an intrasubject registration. Such registration is performed on the T1 images because they show more contrast between tissue classes compared to FLAIR images, and it is aided by a prior lesion filling to avoid a negative impact on registration result due to the presence of WM lesions.

It has been recognized that non-symmetric registration protocols increase the risk of inducing false positive differences, therefore the images of the two time points are aligned to a point that lies in between the space of each lesion map by using the square root of the transformation matrix.

The coregistration algorithm which is exploited by the longitudinal pipeline is the *longitudinal rigid transformation* implemented in the SPM12 toolbox *CAT12*. This

52

algorithm combines rigid-body registration with initial bias field correction and uses sinc interpolation. Coregistration matrices are then applied to corresponding FLAIR images after bias field correction and initial coregistration to the corresponding T1 image.

Once all images are in alignment, a joint lesion map is rendered in order to divide the WM into lesion (part of any lesion, at any time point) and non-lesion voxels (NAWM).

The distribution of FLAIR intensity differences is estimated within the voxels of the NAWM in order to enable statistical quantification of intensity changes within the joint lesion map: significant changes are interpreted as increase (new or enlarged lesion), or decrease (disappeared or shrunken lesion), while non-significant changes are interpreted as lesions at both time points.

A graphic representation of the longitudinal pipeline is presented in figure 2.10[48].
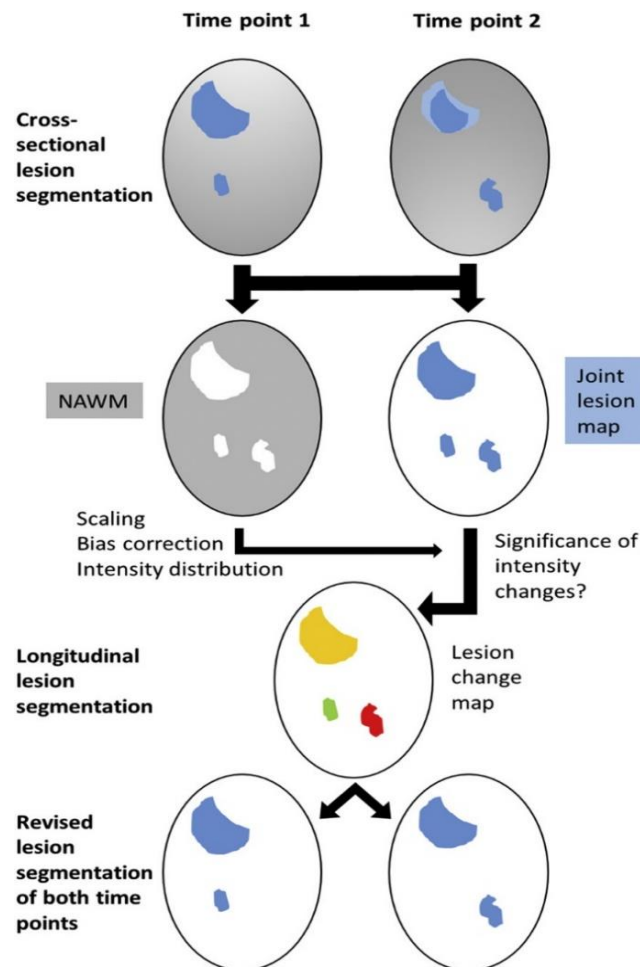
Figure 2.10: LST longitudinal pipeline

The final result is a map called *LCL* (Lesion Change Labels), where the three possible cases decrease, no change and increase are labelled by the numbers 1, 2 and 3, respectively, as well as the corresponding *lrmFLAIR*.

Figure 2.11 shows an example of the LCL mask, where the colour blue represents a decrease of that lesion area between the two time points, the colour orange represents invariance, and the red colour represents an increase.
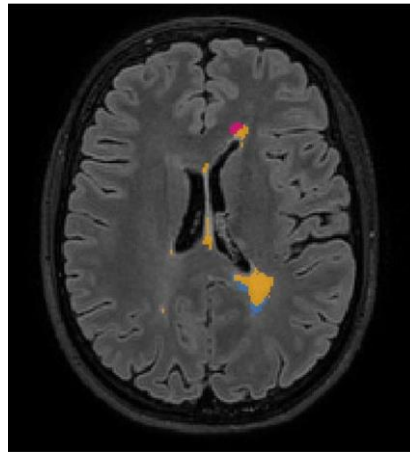
Figure 2.11: Example of LCL mask

2.3.6 QSM data processing

The quantitative measurement of susceptibility was obtained by utilizing *Matlab* toolbox *STI Suite,* which contains both *Matlab* command-line functions and graphical user interfaces for phase processing, QSM, STI and related visualization and ROI analysis tools[57].

The *Read_DICOM_HW* function was employed in order to read the GRE images, which were then separated into magnitude and phase[58]. As described in 1.3.1, the magnitude images were exploited to obtain the mask of the brain tissue by using the *Brain Extraction Tool* (BET) for *FSL* software, while the phase images underwent additional processing steps.

First of all, a Laplacian-based phase unwrapping was performed by using the function *MRPhaseUnwrap.* This method falls under the category of the spatial unwrapping methods, which draw on the fact that the phase changes slowly from voxel to voxel, unless

a wrap has occurred, and it attempts to identify the unwrapped phase whose local derivatives are most similar to the derivates of the wrapped phase[58].

An example of unwrapped phase image of one echo is represented in figure 2.12.
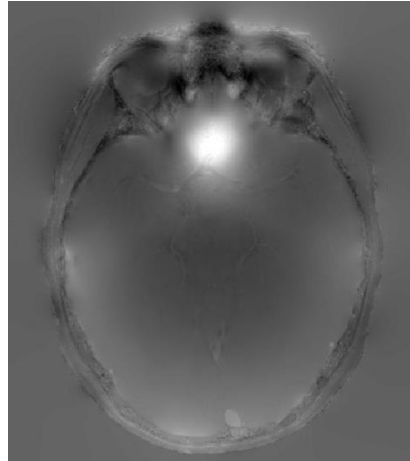
Figure 2.12: Example of unwrapped phase image

The following step was the background phase removal by using the function *V-SHARP*, which requires as inputs both the unwrapped phase and the binary brain mask obtained from the magnitude images, and returns as outputs for each echo the tissue phase and a new mask, slighter smaller than the original one[57].

This function uses a varying spherical kernel to remove the background phase in two passages: first, a new phase is computed by subtracting to the phase itself the value of the convolution between the phase and a *spherical mean value* (SMV) kernel, then the invalid points at the region boundary are removed. The final step is to perform a deconvolution to restore the low frequency tissue phase.

The SMV radius value was set to 4mm, as a compromise between a small SMV value, which has a high devolution power but may cause large amplification of the residual phase error, and a too large diameter, which has a much lower level of phase error but causes a larger boundary regions to be discarded.

Figure 2.13 reports an example of tissue phase of one echo.
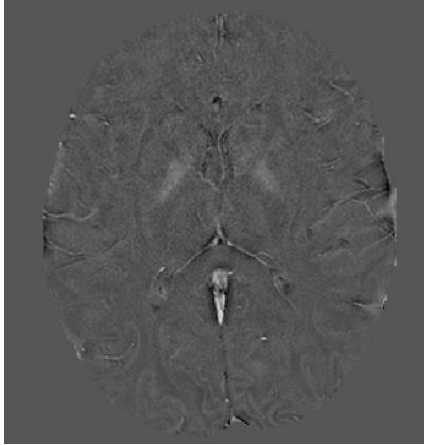
Figure 2.13: Example of tissue phase

Finally, the tissue phase of the six echoes was mediated and given as input to the function *QSM_star,* which implements the *streaking artifacts reduction QSM* (STAR QSM) algorithm. This algorithm is able to reconstruct both large and small susceptibility values using a two levels regularization method: first, the algorithm computes the susceptibility from strong sources, then the field of these sources is estimated and subtracted from the total phase in order to find the susceptibility of the weaker sources. As its name suggests, this method has also been shown to reduce streaking artefacts.

An example of quantitative susceptibility map obtained by using the above written pipeline is reported in figure 2.14.
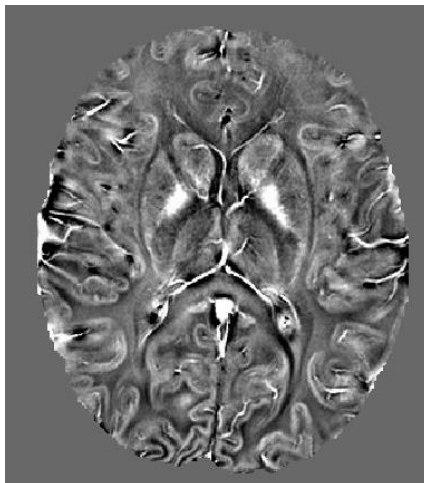
Figure 2.14: Example of QSM image

2.3.7 Volumetric measurements

The *FreeSurfer* function *recon-all,* which was used to segment white matter in an automatic way (see 2.3.2), provides several outputs called *stats.* One of these files was converted by using the function *aparcstats2table* in order to create a table containing for each patient a quantitative measurement of:

- Total WM volume
- Total GM volume
- CSF volume
- Estimated total intracranial volume (eTIV)

For the subsequent statistical analysis, the rough WM and GM volumes were normalized by the eTIV, obtaining what are called *WM fraction* (WMF) and *GM fraction* (GMF). Therefore, they will be expressed in percentage of the TIV.

The NAWM volume, obtained by subtraction of the lesion volume from the WM volume, has been normalized as well in order to obtain the *NAWM fraction* (NAWMF), that will be expressed in percentage of the TIV as well.

2.3.8 Coregistration

Not all the aforementioned processing steps operate in the same space, and even between images that were acquired during the same scan, a coregistration step is often necessary in order to reduce the overlap discrepancies which are due to small movements of the patient between the acquisition of the different sequences. For this reason, a coregistration step was performed in order to further proceed with statistical analysis.

SPM12 function *Coregister (Estimate&Reslice)* was used.

Coregistration requires the setting of three inputs and the interpolation methods: the "reference image" is the image that is assumed to remain stationary while the "source image" is moved to match it, the "source image" is the image that is jiggled about to best match the reference, "other images" are any images that need to remain in alignment with the source image, while the "interpolation" is the method by which the images are sampled while being written in a different space.

2.3.8.1 Coregistration between QSM and FreeSurfer segmentation

The susceptibility maps were obtained from the spoiled GRE multi-echo images, whereas *FreeSurfer* segmentation worked on 3D T1 images. Therefore, a coregistration was performed by setting the 3D T1 image as reference image, the GRE magnitude image as source image and the susceptibility map as other image.
Interpolation was kept at its default option, which is trilinear interpolation.

2.3.8.2 Coregistration of the LCL to the two time points

This step was necessary exclusively for the 13 patients constituting the longitudinal study group.

As described in 2.3.5, the *longitudinal pipeline* implemented by the LST for SPM12 operates on a space that lies in between the spaces of the WML maps and their corresponding *rmFLAIR* images. For this reason, the *lrmFLAIR* was set as source image to be coregistered onto the reference *rmFLAIR* of each time point, together with its correlated LCL map.
In this case, interpolation was set to *nearest neighbour* in order to not create intermediate values in the coregistered LCL map.

2.3.9 Neuroimaging measurements

A ROI-based extraction of the mean QSM value was exploited in *Matlab* for both time points, in order to study susceptibility:

- Inside the normal-appearing white matter, thanks to the overlapping between QSM and the NAWM mask (see 2.3.4)
- Inside the lesions, thanks to the overlapping between QSM and the lesion map (see 2.3.3)
- For the 13 longitudinal patients, inside the disappeared/not changed/increased lesions areas, thanks to the overlapping between QSM and the LCL mask (see 2.3.5)

2.4 Statistical analysis

Statistical Package for Social Science (IBM SPSS statistics, version 26.0.0.0) and *Matlab* (version 2019b) were employed to analyse the data.

The neuroimaging data extracted from the MRI images was combined with clinical variables in order to compare different groups, to look for correlations and to build regression models.

Statistical analysis was divided in statistical analysis of the separate time points groups (G0 and G1) and statistical analysis of the longitudinal study group (at T0 and T1).

2.4.1 Statistical analysis of separate time points groups G0 and G1

Statistical analysis of separate time points refers to analysis that have been done on the whole G0 or G1 study groups, which comprise respectively 38 patients whose magnetic resonance images were acquired within 6 months their diagnosis of multiple sclerosis and 34 patients whose magnetic resonance was acquired at more than 6 months from their diagnosis of multiple sclerosis.

2.4.1.1 Age, disease duration, sex comparison among groups

Group differences in age and disease duration were evaluated with Mann-Whitney tests. They were assessed between the whole G0 and G1 study groups and then within each group, among RR patients and P patients.

Group differences in sex were evaluated with chi-squared (χ^2) tests, both between the whole G0 and G1 study groups and within each group, among RR patients and P patients.

In case some parameters showed a statistically significant difference between groups, they were included as confounding factors in the subsequent statistical analysis.

2.4.1.2 Descriptive statistics

Descriptive statistics were analysed in order to have an overview on the median, the interquartile range, the minimum value and the maximum value of the neuroimaging measurements.

2.4.1.3 Neuroimaging measurement analysis

Wilcoxon tests (rank-based non-parametric test) and Mann Whitney tests (rank-based non-parametric test) were employed in order to perform a univariate comparison of the neuroimaging measurements, namely the mean value of susceptibility in the NAWM and inside the lesions.

The former is a statistical test which is utilized to compare two sets of data that come from the same group, while the latter is used when the two groups whose data is analysed are independent.

2.4.1.4 Neuroimaging measurements and clinical variables correlations

Spearman's correlation tests were performed between relevant neuroimaging measurements (mean value of susceptibility inside the NAWM and the lesions at T0, GMF and NAWM at T0) and the difference on the EDSS score between the two time points. The correlation between the mean value of susceptibility inside the NAWM and the difference on the EDSS score between the two time points was the most significant correlation from a clinical point of view and it was used as starting point for the building of multiple regression prediction models.

2.4.1.5 Multiple regression analysis of clinical variables

Two multiple regression models were created in order to predict the difference on the EDSS score between the two time points. The statistically significant predictor for both models was the mean value of susceptibility inside the NAWM, but the second model also included the lesion volume at T0, which was demonstrated to have a borderline statistical significance.

2.4.2 Statistical analysis of the longitudinal study group

Statistical analysis of the longitudinal study group refers to analysis that have been performed on the 13 patients whose magnetic resonance images was available both at time T0 and at time T1, meaning that their magnetic resonance images were acquired both within 6 months their diagnosis of multiple sclerosis and at more than 6 months from their diagnosis of multiple sclerosis.

2.4.2.1 Descriptive statistics

Descriptive statistics were analysed in order to have an overview on the median, the interquartile range, the minimum value and the maximum value of the neuroimaging measurements.

2.4.2.2 Neuroimaging measurement analysis

Wilcoxon tests (rank-based non-parametric test) were employed in order to perform a univariate comparison of neuroimaging measurements, since analysed data came from the same group.

2.4.2.3 Neuroimaging measurements and clinical variables correlations

Spearman's correlation tests were performed between relevant neuroimaging measurements (mean value of susceptibility inside the NAWM and the lesions at T0 and T1, GMF and NAWM at T0 and T1) and clinical variables (difference on the EDSS score between the two time points and EDSS score at T1).

The most significant correlations from a clinical point of view, which are the correlations between the mean value of susceptibility inside the NAWM and the GMF at both time points, were used as starting point for the building of multiple regression prediction models.

2.4.2.4 Multiple regression analysis of clinical variables

Two multiple regression models were created in order to predict respectively the GMF at T0 and T1 by using as predictors the mean value of susceptibility inside the NAWM and the lesion volume at T0, both showing a statistical significance.

Chapter 3

Results

Results are divided in two main parts: statistical analysis of separate time point groups (G0 and G1) and statistical analysis of the longitudinal study group (at T0 and T1). For what concerns the statistical analysis of separate time point groups, results of age, disease duration and sex differences among groups are reported. Then, results of statistical tests on neuroimaging measurements are presented along with results of correlation and regression analysis among neuroimaging measurements and clinical variables.

Regarding the statistical analysis of the longitudinal study group, it comprises statistical tests on neuroimaging measurements, as well as correlation and regression analysis.

3.1 Statistical analysis of separate time points groups G0 and G1

This section presents the results of statistical analysis that were conducted separately for the G0 group and/or for the G1 group.

3.1.1 Age differences among groups

The statistical significance of age was evaluated between the two time point groups with a Mann-Whitney test and it resulted negligible (U = 485.5, p = 0.070).

Age was also evaluated separately for the two time point groups between RR patients and P patients, showing a statistical difference both in G0 patients (U = 15.0, p = 0.000) and in G1 patients (U = 33.0, p = 0.001).

3.1.2 Sex differences among groups

Sex was evaluated between the two time points and it did not show any statistical significance ($\chi^2(1)$ = 0.126, p = 0.723).

Sex was also evaluated separately for the two time point groups between RR patients and P patients. It did not statistically differ neither in G0 patients ($\chi^2(1)$ = 3.335, p = 0.068) nor in G1 patients ($\chi^2(1)$ = 0.200, p = 0.655).

3.1.3 Disease duration differences among groups

Disease duration (measured in months) was evaluated between the two time point groups with a Mann-Whitney test, showing a statistical significance (U = 8.0, p = 0.000).

Disease duration was also evaluated separately for the two time point groups between RR patients and P patient. Disease duration at T0 did not statistically differ neither in G0 patients (U = 92.5, p = 0.882) nor in G1 patients (U = 103.0, p = 0.706). Disease duration at T1 did statistically differ in G0 patients (U = 44.5, p = 0.037) but it did not in G1 patients (U = 110.5, p = 0.939).

3.1.4 Descriptive statistics

In the following paragraphs, some descriptive statistics are presented in order to provide an overview of the neuroimaging measurements characteristics. In particular, descriptive statistics of the mean value of susceptibility in the NAWM and inside the lesions are reported for both time point groups.

3.1.4.1 Descriptive statistics of NAWM susceptibility

Descriptive statistics of the mean value of susceptibility inside the NAWM both for group G0 (QSM NAWM G0) and for group G1 (QSM NAWM G1) are reported in table 3.1.

	Median	Interquartile range	Minimum	Maximum
QSM NAWM G0	-0,00231	-0,00249 - -0,00197	-0,00282	-0,00073
QSM NAWM G1	-0,00217	-0,00248 - -0,00182	-0,00283	-0,00130

Table 3.1: Descriptive statistics of NAWM susceptibility

3.1.4.2 Descriptive statistics of lesions susceptibility

Descriptive statistics of the mean value of susceptibility inside the lesions both for group G0 (QSM lesions G0) and for group G1 (QSM lesions G1) are reported in table 3.2.

	Median	Interquartile range	Minimum	Maximum
QSM lesions G0	0,00200	0,00062 - 0,04094	-0,00305	0,01087
QSM lesions G1	0,00219	0,00125 - 0,00357	-0,00079	0,00972

Table 3.2: Descriptive statistics of lesions susceptibility

3.1.5 Neuroimaging measurement analysis

The following paragraphs report the results of statistical tests on neuroimaging measurements.

3.1.5.1 NAWM susceptibility comparison among time point groups (G0-G1)

The differences on the mean value of susceptibility in the NAWM were evaluated among the two time point groups G0 and G1 with a Mann-Whitney test, showing no statistical significance (U = 558.0, p = 0.321).

3.1.5.2 Lesions susceptibility comparison among time point groups (G0-G1)

The differences on the mean value of susceptibility inside the lesions were evaluated among the two time point groups G0 and G1 with a Mann-Whitney test, showing no statistical significance (U = 640.0, p = 0.946).

3.1.5.3 NAWM and lesion susceptibility comparison (G0)

The differences between the mean value of susceptibility in the NAWM and inside the lesions within the same group of patients were evaluated for the group G0 with a Wilcoxon test.

The mean value of susceptibility inside the lesions resulted to be greater than the mean value of susceptibility in the NAWM with statistical significance (Z = -5.243, p = 0.000).

3.1.5.4 NAWM and lesion susceptibility comparison (G1)

The differences between the mean value of susceptibility in the NAWM and inside the lesions within the same group of patients were evaluated for the group G1 with a Wilcoxon test.

The mean value of susceptibility inside the lesions resulted to be greater than the mean value of susceptibility in the NAWM with statistical significance (Z = -5.086, p = 0.000).

3.1.5.5 NAWM susceptibility comparison between RR and P patients (G0)

The differences on the mean value of susceptibility in the NAWM were evaluated within the same time point group between RR patients and P patients with a Mann-Whitney test.

For the G0 time point group, the mean value of susceptibility in the NAWM in P patients resulted to be greater than the mean value of susceptibility in the NAWM in RR patients with statistical significance (U = 35.0, p = 0.015).

3.1.5.6 NAWM susceptibility comparison between RR and P patients (G1)

The differences on the mean value of susceptibility in the NAWM were evaluated within the same time point group between RR patients and P patients with a Mann-Whitney test.

For the G1 time point group, the mean value of susceptibility in the NAWM in P patients resulted to be greater than the mean value of susceptibility in the NAWM in RR patients with statistical significance (U = 39.0, p = 0.004).

3.1.6 Neuroimaging measurements and clinical variables correlation

The following paragraph reports the results of correlation tests between neuroimaging measurements and clinical variables.

3.1.6.1 Correlations for the NAWM and lesions susceptibility (G0)

The results of correlation tests for the group G0 between the mean susceptibility inside the NAW, the mean susceptibility inside the lesions, the GMF, the NAWMF and the ΔEDSS (the difference of the EDSS scores between the two time points in which the EDSS was evaluated) are reported in table 3.3.

Significance is highlighted with different colours according to its value: yellow for values ≤ 0.05, orange for values ≤ 0.01. Correlation is marked with one asterisk (*) when it is significant at the 0.05 level, and with two asterisks (**) when it is significant at the 0.01 level.

Correlations		QSM NAWM G0	QSM lesions G0	GMF G0	NAWMF G0	DeltaEDSS
QSM NAWM G0	**Correlation Coefficient**	1,000	-0,089	$-,518^{**}$	$-,493^{**}$	$,489^{**}$
	p	/	0,597	0,001	0,002	0,002
QSM lesions G0	**Correlation Coefficient**	/	1,000	$,366^{*}$	0,259	-0,162
	p	/	/	0,026	0,121	0,330
GMF G0	**Correlation Coefficient**	/	/	1,000	$,726^{**}$	$-,571^{**}$
	p	/	/	/	0,000	0,000
NAWMF G0	**Correlation Coefficient**	/	/	/	1,000	$-,522^{**}$
	p	/	/	/	/	0,001
DeltaEDSS	**Correlation Coefficient**	/	/	/	/	1,000
	p	/	/	/	/	/

Table 3.3: Correlations for the NAWM and lesions susceptibility

3.1.7 Multiple regression analysis of clinical variables

The following paragraphs report the result of two multiple regression models that have been created in order to predict the ΔEDSS between the two time points, the first one being based exclusively on the mean value of susceptibility in the NAWM, the second one being based on the lesions volume as well.

3.1.7.1 Multiple regression of ΔEDSS on NAWM susceptibility

A multiple regression model has been created for the group G0 in order to predict the ΔEDSS (the difference of the EDSS scores between the two time points in which the EDSS was evaluated) by using as independent variables the mean value of susceptibility inside the NAWM, the age, the sex and the disease duration at T1.

These variables statistically significantly predicted the ΔEDSS ($F(4,33) = 2.914$, $p = 0.036$, $R^2 = 0.261$), but only the mean value of susceptibility in the NAWM added statistically significantly to the prediction ($p = 0.015$), while the other independent variables did not show a significant p-value ($p = 0.278$, $p = 0.983$, $p = 0.956$ respectively). A plot graphically shows the relationship between the variables used as predictors and the dependent variable in figure 3.1.

Figure 3.1: Multiple regression plot of ΔEDSS on QSM NAWM G0, age, sex and disease duration at T1

3.1.7.2 Multiple regression of ΔEDSS on NAWM susceptibility and lesion volume

A multiple regression model has been created for the group G0 in order to predict the ΔEDSS (the difference of the EDSS scores between the two time points in which the EDSS was evaluated) by using as independent variables the mean value of susceptibility inside the NAWM, the volume of WM lesions, the age, the sex and the disease duration at T1.

These variables statistically significantly predicted the ΔEDSS ($F(5,30) = 3.141$, $p = 0.021$, $R^2 = 0.344$), but only the mean value of susceptibility in the NAWM added statistically significantly to the prediction ($p = 0.019$), while the volume of WM lesions resulted to have a borderline significance ($p = 0.051$) and the other independent variables did not show a significant *p-value* ($p = 0.743$, $p = 0.423$, $p = 0.833$ respectively).

A plot graphically shows the relationship between the variables used as predictors and the dependent variable in figure 3.2.
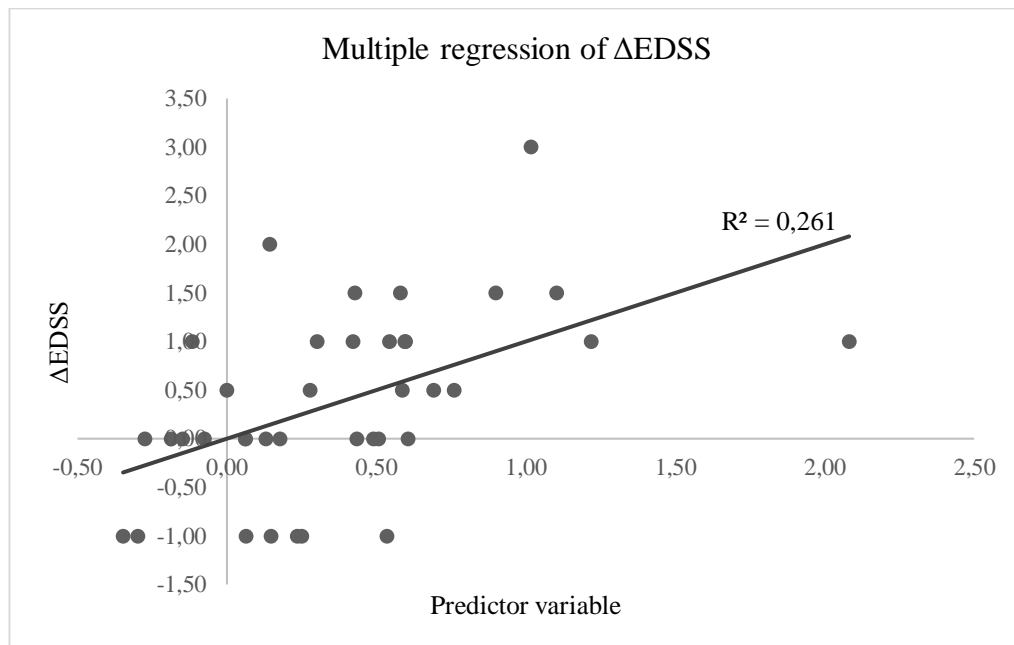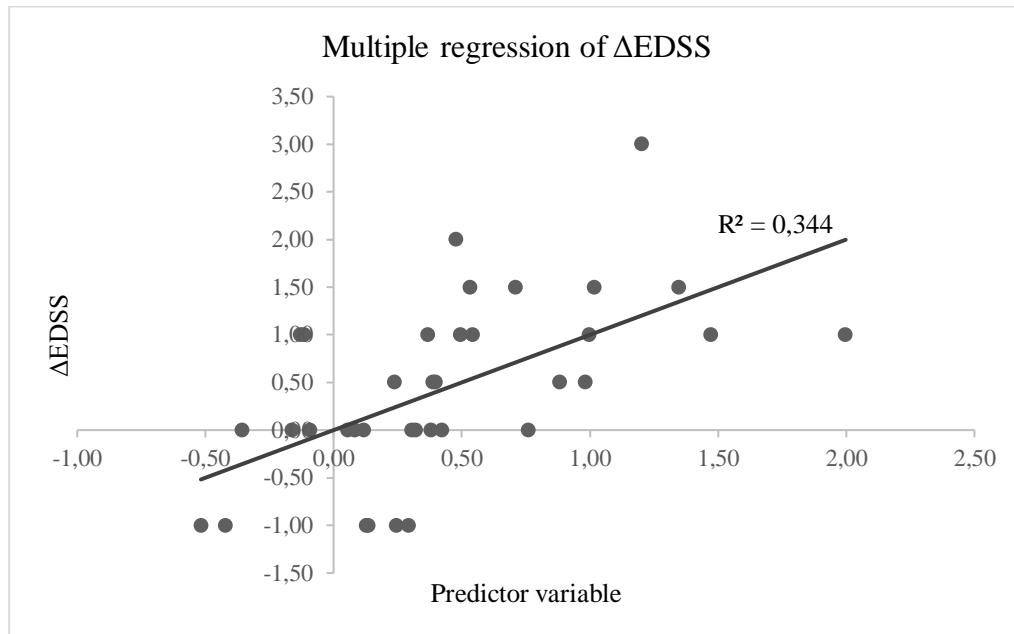

Figure 3.2: Multiple regression plot of ΔEDSS on QSM NAWM G0, WM lesion volume, age, sex and disease duration at T1

3.2 Statistical analysis of the longitudinal study group

This section presents the results of statistical analysis that were conducted for the patients whose resonance magnetic data was acquired at both T0 and T1 time points.

The number of these patients was 13, but because of some incongruences a subject was removed from the statistical analysis regarding the GMF.

3.2.1 Descriptive statistics

In the following paragraphs, some descriptive statistics are presented in order to provide an overview of the neuroimaging measurements characteristics. In particular, descriptive statistics of the mean susceptibility value of the NAWM, inside the lesions and inside the decreased/not changed/increased lesion areas are reported for both time points.

3.2.1.1 Descriptive statistics of NAWM susceptibility

Descriptive statistics of the mean value of susceptibility inside the NAWM both at time T0 (QSM NAWM T0) and at time T1 (QSM NAWM T1) are reported in table 3.4.

	Median	Interquartile range	Minimum	Maximum
QSM NAWM T0	-0,00215	-0,00249 - -0,00194	-0,00273	-0,00155
QSM NAWM T1	-0,00216	-0,00244 - -0,00185	-0,00276	-0,00149

Table 3.4: Descriptive statistics of NAWM susceptibility

3.2.1.2 Descriptive statistics of lesions susceptibility (T0)

Descriptive statistics of the mean value of susceptibility inside the lesions at T0 (QSM lesions T0) are reported in table 3.5. This table also reports the mean value of susceptibility inside the lesion areas labelled as decreased (1), not changed (2) and increased (3) between the two time points by the LCL. This means that at T0:

- Label 1 represents a lesion area that is going to heal at T1
- Label 2 represents a lesion area that is not going to change at T1
- Label 3 represents an area where a lesion is going to appear at T1

	Median	Interquartile range	Minimum	Maximum
QSM lesions T0	0,00134	0,00107 - 0,00353	0,00005	0,00491
QSM label1 T0	-0,00356	-0,00812 - 0,00036	-0,02124	0,00674
QSM label2 T0	0,00122	0,00028 - 0,00288	-0,00058	0,00386
QSM label3 T0	0,00299	-0,00605 - 0,00612	-0,01118	0,01503

Table 3.5: Descriptive statistics of susceptibility inside the lesions and inside the lesion areas labelled as 1,2,3 at T0

3.2.1.3 Descriptive statistics of lesions susceptibility (T1)

Descriptive statistics of the mean value of susceptibility inside the lesions at T1 (QSM lesions T1) are reported in table 3.6. This table also reports the mean value of susceptibility inside the lesion areas labelled as decreased (1), not changed (2) and increased (3) between the two time points by the LCL. This means that at T1:

- Label 1 represents an area that has healed with respect to T0
- Label 2 represents a lesion area that has not changed with respect to T0
- Label 3 represents a lesion area that has appeared at T1 but was not present at T0

	Median	Interquartile range	Minimum	Maximum
QSM lesions T1	0,00152	0,00084 - 0,00346	-0,00030	0,00481
QSM label1 T1	-0,00053	-0,00629 - 0,00097	-0,04354	0,00281
QSM label2 T1	0,00098	0,00031 - 0,00299	-0,00074	0,00335
QSM label3 T1	0,00112	-0,00382 - 0,00977	-0,00738	0,02290

Table 3.6: Descriptive statistics of susceptibility inside the lesions and inside the lesion areas labelled as 1,2,3 at T1

3.2.2 Neuroimaging measurements analysis

3.2.2.1 Labels susceptibility comparison (T0)

The differences between the mean value of susceptibility in the different labels within the same time point were evaluated with a Wilcoxon test.

At time point T0, the mean value of susceptibility in label 2 resulted to be greater than the mean value of susceptibility in label 1 with statistical significance ($Z = -2.312$, $p = 0.021$).
On the contrary, the differences between label 3 and label 1 and between label 3 and label 2 did not show a statistical significance ($Z = -1.423$, $p = 0.155$ and $Z = -0.392$, $p = 0.695$ respectively).

3.2.2.2 Labels susceptibility comparison (T1)

The differences between the mean value of susceptibility in the different labels within the same time point were evaluated with a Wilcoxon test.

At time point T1, the mean value of susceptibility in label 2 resulted to be greater than the mean value of susceptibility in label 1 with statistical significance ($Z = -2.578$, $p = 0.010$), and the mean value of susceptibility in label 3 resulted to be greater than the mean value of susceptibility in label 1 with statistical significance ($Z = -2.045$, $p = 0.041$).
On the contrary, the differences between label 3 and label 2 did not show a statistical significance ($Z = -0.314$, $p = 0.754$).

3.2.3 Neuroimaging measurements and clinical variables correlations

The following paragraph reports the results of correlation tests between neuroimaging measurements and clinical variables.

3.2.3.1 Correlations between NAWM susceptibility, lesions susceptibility and EDSS

The results of the correlation tests between the mean susceptibility inside the NAWM at T0 and T1, the mean susceptibility inside the lesions at T0 and T1, the EDSS score at T1 and the difference on the EDSS score between the two time points are reported in table 3.7.

Significance is highlighted with different colours according to its value: yellow for values ≤ 0.05, orange for values ≤ 0.01. Correlation is marked with one asterisk (*) when it is significant at the 0.05 level, and with two asterisks (**) when it is significant at the 0.01 level.

Correlations		QSM NAWM T0	QSM NAWM T1	QSM lesions T0	QSM lesions T1	Delta EDSS	EDSS al T1
QSM NAWM T0	**Correlation Coefficient**	1,000	,868**	-0,401	-0,341	,593*	,777**
	p	/	0,000	0,174	0,255	0,033	0,002
QSM NAWM T1	**Correlation Coefficient**	/	1,000	-0,209	-0,165	0,450	,851**
	p	/	/	0,494	0,590	0,123	0,000
QSM lesions T0	**Correlation Coefficient**	/	/	1,000	,775**	0,265	-0,265
	p	/	/	/	0,002	0,381	0,382
QSM lesions T1	**Correlation Coefficient**	/	/	/	1,000	0,250	-0,191
	p	/	/	/	/	0,409	0,533
Delta EDSS	**Correlation Coefficient**	/	/	/	/	1,000	0,491
	p	/	/	/	/	/	0,088
EDSS at T1	**Correlation Coefficient**	/	/	/	/	/	1,000
	p	/	/	/	/	/	/

Table 3.7: Correlations between NAWM susceptibility, lesions susceptibility and EDSS

3.2.3.2 Correlations between NAWM susceptibility, volumetric measurements and EDSS

The results of correlation tests between the mean susceptibility inside the NAWM at T0 and T1, its difference between the two time points, the difference on the EDSS score between the two time points, the GMF and the NAWMF at both time points are reported in table 3.8.

Significance is highlighted with different colours according to its value: yellow for values ≤ 0.05, orange for values ≤ 0.01. Correlation is marked with one asterisk (*) when it is significant at the 0.05 level, and with two asterisks (**) when it is significant at the 0.01 level.

Correlations		QSM NAWM T0	QSM NAWM T1	Delta QSM	Delta EDSS	GMF T0	GMF T1	NAWMF T0	NAWMF T1
Mean QSM NAWM T0	Correlation Coefficient	1,000	,868**	0,055	,593*	-,734**	-,725**	-0,517	-0,511
	p	/	0,000	0,881	0,033	0,007	0,005	0,085	0,074
QSM NAWM T1	Correlation Coefficient	/	1,000	0,588	0,450	-0,573	-,604*	-0,566	-0,511
	p	/	/	0,074	0,123	0,051	0,029	0,055	0,074
Delta QSM	Correlation Coefficient	/	/	1,000	-0,201	-0,176	-0,176	-0,479	-0,358
	p	/	/	/	0,578	0,627	0,627	0,162	0,310
Delta EDSS	Correlation Coefficient	/	/	/	1,000	-0,377	-0,277	-0,189	-0,104
	p	/	/	/	/	0,227	0,359	0,557	0,734
GMF T0	Correlation Coefficient	/	/	/	/	1,000	1,000**	,811**	,832**
	p	/	/	/	/	/	0,000	0,001	0,001
GMF T1	Correlation Coefficient	/	/	/	/	/	1,000	,811**	,846**
	p	/	/	/	/	/	/	0,001	0,000
NAWMF T0	Correlation Coefficient	/	/	/	/	/	/	1,000	,958**
	p	/	/	/	/	/	/	/	0,000
NAWMF T1	Correlation Coefficient	/	/	/	/	/	/	/	1,000
	p	/	/	/	/	/	/	/	/

Table 3.8: Correlations between NAWM susceptibility, volumetric measurements and EDSS

3.2.4 Multiple regression analysis of clinical variables

The following paragraphs report the result of two multiple regression models that have been created in order to predict the GMF at both time points, based on the mean value of susceptibility inside the NAWM and on the lesions volume at T0.

3.2.4.1 Multiple regression of GMF T0 on NAWM susceptibility and lesions volume

A multiple regression model has been created for in order to predict the GMF at T0 by using as independent variables the mean value of susceptibility in the NAWM at T0, the volume of WM lesions at T0, the age and the sex.

These variables statistically significantly predicted the ΔEDSS ($F(4,7) = 8.646$, $p = 0.008$, $R^2 = 0.832$), but only the mean value of susceptibility in the NAWM at T0 and the volume of WM lesions at T0 added statistically significantly to the prediction ($p = 0.015$ and $p = 0.034$, respectively), while the other independent variables did not show a significant *p-value* ($p = 0.081$, $p = 0.498$ respectively).

A plot graphically shows the relationship between the variables used as predictors and the dependent variable in figure 3.3.

Figure 3.3: Multiple regression plot of GMF T0 on QSM NAWM T0, age, sex and lesions volume at T0

3.2.4.2 Multiple regression of GMF T1 on NAWM susceptibility and lesions volume

A multiple regression model has been created in order to predict the GMF at T1 by using as independent variables the mean value of susceptibility in the NAWM at T0, the volume of WM lesions at T0, the age and the sex.

These variables statistically significantly predicted the ΔEDSS ($F(4,7) = 5.935$, $p = 0.021$, $R^2 = 0.772$), but only the mean value of susceptibility in the NAWM at T0 added statistically significantly to the prediction ($p = 0.045$), while the volume of WM lesions at T0 showed a borderline significance ($p = 0.053$) and the other independent variables did not show a significant *p-value* ($p = 0.117$ and $p = 0.493$ respectively).

A plot graphically shows the relationship between the variables used as predictors and the dependent variable in figure 3.4.
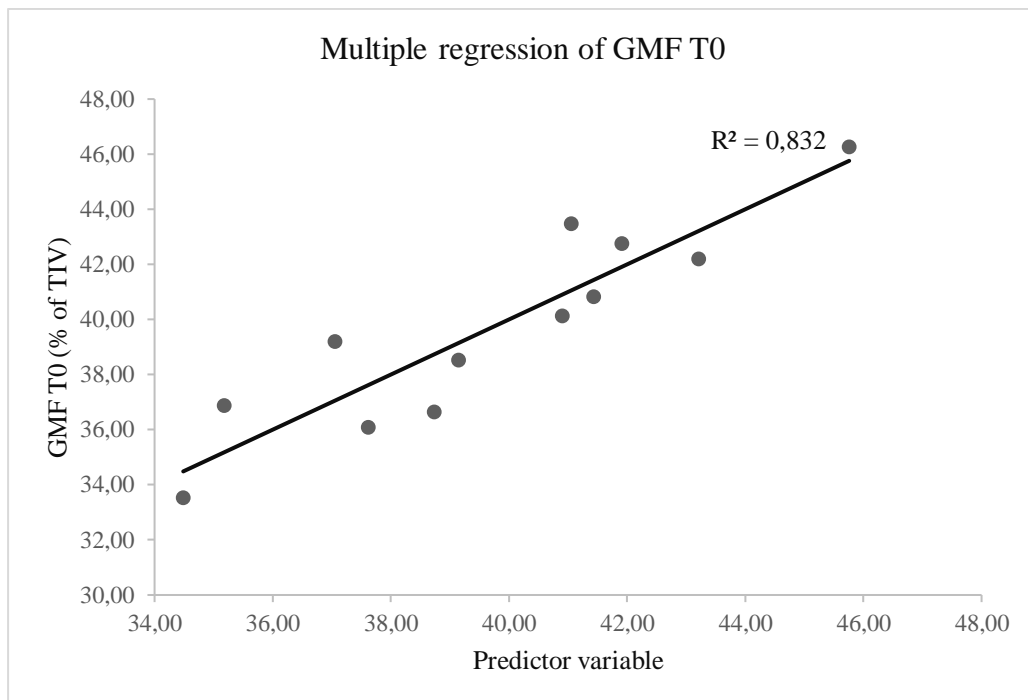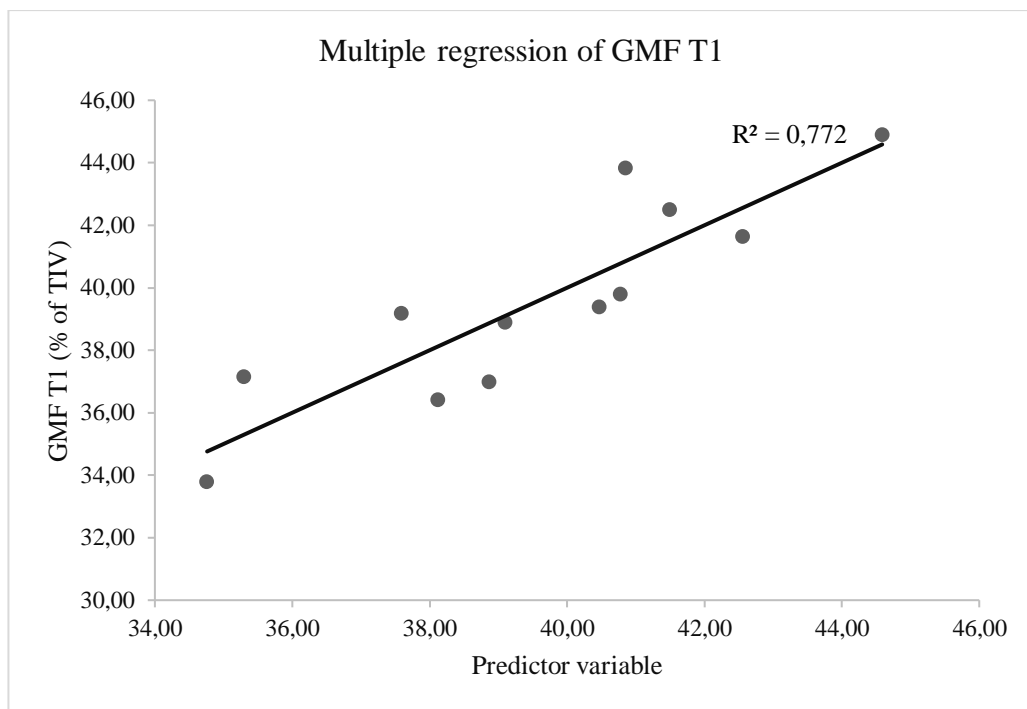

Figure 3.4: Multiple regression plot of GMF T1 on QSM NAWM T0, age, sex and lesions volume at T0

Chapter 4

Discussion

The quantification of susceptibility in brain tissues in multiple sclerosis patients have become object of relevant interest for the definition of premature signs of the disease onset and development[39]. However, studies have been focused on the deep grey matter, whereas histopathological examinations and *in vivo* MR techniques have suggested that the white matter is affected by the disease not only by the presence of lesions, but also by pathological changes in the NAWM. These abnormalities, which comprise axonal degeneration[63], microglia and astroglia proliferation[64], demyelination and structural changes[62], seem to start from the earliest stages of the disease, but they are not visible in conventional MR images.

For these reasons, assessing susceptibility in the NAWM with a non-invasive processing of GRE images might be a promising tool for a deeper understanding of the underlying pathological changes and to find a correlation between the imaging measurement and the effective functional state of individuals.

In this thesis, the primary aim was the assessment of magnetic susceptibility in the NAWM in patients with multiple sclerosis. A characterization of the lesions by volumetry and Quantitative Susceptibility Mapping and the evaluation of the changes in susceptibility between two time point groups (G0 and G1) and within the same sample of patient in two different time points (T0 and T1) were performed as well.

The neuroimaging measurement that was extracted from these ROIs in both pipelines was the mean value of susceptibility, which was integrated with volumetric information of the different cerebral tissues and with clinical information regarding the degree of disability and the duration of the disease. In the following discussion, the most significant results from a clinical point of view will be reviewed and assessed.

For what concerns statistical analysis of separate time points, a statistically significant difference on the mean value of susceptibility among the NAWM and the

lesions for both time point groups was highlighted, supporting the hypothesis that demyelination processes[37] and iron laden microglia at the lesion borders[36] might be the cause of an increased susceptibility inside the lesion tissues.

However, the mean value of susceptibility in the NAWM might constitute an aid for MS diagnosis, since there is a statistically significant difference of its value between the RR patients and P patients already at an early stage of the disease (group G0), which becomes even more significant as the disease progresses (group G1). Indeed, P patients features a higher susceptibility in the NAWM compared to RR patients, which may be explained with higher and ongoing inflammation and demyelination processes.

The most relevant correlation results are the statistically significant correlations for group G0 between the mean value of susceptibility in the NAWM and the NAWMF, the GMF and the ΔEDSS. While the first one implies a relationship between susceptibility and atrophy in the same tissue at the same time point, the second and the third ones confirm the link between GM atrophy and disability[52][53] and suggest a strong connection between the NAWM susceptibility and the disease progression.
On the contrary, even if the mean value of susceptibility inside the lesions correlates with the GMF at the same time point, it does not correlate with the NAWM atrophy and it is not able to forecast the difference on the EDSS score between the two time points either, as stated in literature[42].

The promising correlation between the mean value of susceptibility in the NAWM and the ΔEDSS has been exploited in order to build two multiple regression models, which may be meaningful for the clinical practice as they are able to predict in a statistically significant way the temporal course of disability as a function of the susceptibility itself.
The first model is already significant and employs as independent variable the mean value of susceptibility in the NAWM, together with age, sex and disease duration at T1. Nevertheless, the R-squared value, which indicates how much of the total variation in the dependent variable can be explained by the dependent variable, results pretty low.
By adding to the predictors the volumetric measure of WM lesions, the model increases in statistical significance and data fitting, being the WM lesions volume a borderline significant predictor of the ΔEDSS as well.

Regarding the longitudinal study group, the investigation on the mean value of susceptibility in the decreased/not changed/increased lesion areas at time point T0 has shown a statistically significant difference between label 1 and label 2, meaning that lesion areas that are going to disappear at T1 (label 1) feature a lower susceptibility at T0 compared to lesion areas that are not going to change between the two time points (label 2). The difference on the value of these labels increases in significance at time point T1: lesion areas that have healed at T1 (label 1) have a lower susceptibility with respect to lesions areas that have not changed from the previous time point. This confirms again the hypothesis of higher susceptibility inside the lesions but, most importantly, claims that inflammation resolution and remyelination actually restore a lower value of susceptibility in the lesion tissues that are going to heal, already at T0.

Correlations for the longitudinal study group not only validate the statistically significant connection of the mean value of susceptibility in the NAWM with the ΔEDSS and the GMF at the same time point, but also show that there is an even more significant correlation between the mean value of susceptibility in the NAWM at T0 and the GMF at T1, suggesting a role of the NAWM susceptibility in predicting the time course of brain atrophy.

Indeed, the two multiple regression models having as independent variables the mean value of susceptibility in the NAWM, the lesion volume at T0, age and sex and as dependent variable the GMF at T0 and T1 respectively have been shown to have a statistical significance and a high value of the R-squared.

Our study demonstrated the validity of the mean value of susceptibility in the NAWM as a neuroimaging measurement which might be potentially able to support the diagnosis process and to prognosticate the course of the disease, namely the brain atrophy in the GM and the progress of disability, in a completely non-invasive way. A relevant aspect of this work is indeed the capability of extrapolating pieces of information about the pathologic condition of a tissue which seems normal when analysed with conventional MR sequences.

Moreover, the study has been conducted by exploiting routine magnetic resonance, thus it did not require additional costs and resources to be employed with respect to the standard clinical practice.

Other important features of this work are the quantitative nature of the study, which overcomes the limits of the other *in vivo* MR techniques that have attempted to be used for the assessment of susceptibility and of the NAWM abnormalities[62][63][64], and the automatic segmentation of the subcortical WM[61], which overcomes the limit of operator-dependency and allows the reproducibility of the study even on large scales.

However, some limitations need to be acknowledged.

A manual refinement was necessary in order to obtain precise WML masks. Nonetheless, the majority of the lesions was detected in an accurate way by the automatic segmentation, making the manual intervention a much less time-consuming process with respect to a fully manual segmentation of lesions.

The lack of a control group to compare our study groups with may be considered as a constraint. On the other hand, MS diagnosis with McDonald criteria is quite straightforward, hence, in the clinical practice, being able to forecast the time course of the disease might be more convenient with respect to aiding the diagnosis of an already forthright standard.

Another limitation is intrinsic to the Quantitative Susceptibility Mapping itself, since the computation of QSM is affected by the assumption that susceptibility is isotropic, whereas it has been demonstrated that some molecules, such as lipids in myelin, have an anisotropic susceptibility which can be described by a susceptibility tensor.

This novel application called *Susceptibility Tensor Imaging* (STI) could be the basis for a future improvement of the study: this would allow not only to quantify the value of susceptibility inside the tissues of interest, but also to assess the orientation of the magnetization of such tissues when exposed to a magnetic field, constituting an even more complete study of the characteristics of the pathological brain.

Another piece of information that might be added to the present study is the analysis of MS biomarkers and the mutual correlation with our neuroimaging measurements and clinical variables, which would render our study a multimodal one.

A larger group of patients should be recruited for the longitudinal study, and more time points might be taken into consideration as well. If compatible with the clinical practice, the first time point might be set earlier in order to further explore the predictive features of the neuroimaging measurements, while the successive time points might be defined in stricter time intervals in order to define a more standardized protocol.

Considering the amount of neuroimaging measurements and clinical variables, once large group of patients are reached, another future improvement may be the employment of machine learning algorithms in order to obtain clinical classifiers and to build other predictive models for the diagnosis and prognosis of MS[59][60].

By exploiting this improvement of the study and the automaticity of the pipeline, a clinical decision support system may be implemented as well, in order to aid neurologists in their clinical practice.

Chapter 5

Conclusions

Two neuroimaging pipelines were implemented in order to primarily assess the magnetic susceptibility in the NAWM in patients with multiple sclerosis. A characterization of the WM lesions by volumetry and by Quantitative Susceptibility Mapping and an evaluation of the changes in susceptibility between two time point groups (G0 and G1) and within the same sample of patients in two different time points (T0 and T1) were performed as well.

The study highlighted the validity of the mean value of susceptibility in the NAWM as a neuroimaging measurement which is potentially able to support diagnosis and to prognosticate the course of the disease: this value have been demonstrated to be significantly higher in progressive patients with respect to relapsing-remitting patients in both time point groups, and has been found to correlate both with brain atrophy measurements (NAWMF and GMF) and with disability measurements (ΔEDSS).

The statistical analysis of the longitudinal study group has further confirmed the correlations of the mean value of susceptibility in the NAWM with brain atrophy measurements (GMF) and disability measurements (ΔEDSS).

Since QSM is possibly sensitive to tissue characteristics specific to the different time points and phenotypes of MS, larger studies are encouraged to validate its utility.

The current thesis work might be further improved with the application of different MRI modalities and through the extension of the study group and the time points, and eventually with the deployment of machine learning algorithms. Multi-modal studies on the NAWM are also suggested in order to provide a more complete characterization of this tissue in MS. By exploiting these improvements, a clinical decision support system might also be implemented in order to aid the clinical practice.

References

[1] Karussis D. *The diagnosis of multiple sclerosis and the various related demyelinating syndromes: a critical review*. J Autoimmun. 2014 Feb-Mar;48-49:134-42.

[2] Dobson R, Giovannoni G. *Multiple sclerosis - a review*. Eur J Neurol. 2019 Jan;26(1):27-40.

[3] Leray E, Yaouanq J, Le Page E, Coustans M, Laplaud D, Oger J, Edan G. *Evidence for a two-stage disability progression in multiple sclerosis*. Brain. 2010 Jul;133(Pt 7):1900-13.

[4] Frohman EM, Racke MK, Raine CS. *Multiple sclerosis-the plaque and its pathogenesis*. N Engl J Med. 2006 Mar 2;354(9):942-55.

[5] Allegretta M, Nicklas JA, Sriram S, Albertini RJ. *T cells responsive to myelin basic protein in patients with multiple sclerosis*. Science. 1990 Feb 9;247(4943):718-21.

[6] Zhang J, Markovic-Plese S, Lacet B, Raus J, Weiner HL, Hafler DA. *Increased frequency of interleukin 2-responsive T cells specific for myelin basic protein and proteolipid protein in peripheral blood and cerebrospinal fluid of patients with multiple sclerosis*. J Exp Med. 1994 Mar 1;179(3):973-84.

[7] Venken K, Hellings N, Hensen K, Rummens JL, Stinissen P. *Memory CD4+CD127high T cells from patients with multiple sclerosis produce IL-17 in response to myelin antigens*. J Neuroimmunol. 2010 Sep 14;226(1e2): 185-91.

[8] Aktas O, Wattjes MP, Stangel M, Hartung HP. *Diagnosis of multiple sclerosis: revision of the McDonald criteria 2017*. Nervenarzt. 2018 Dec;89(12):1344-1354.

[9] Jacobs L, Kinkel PR, Kinkel WR. *Impact of nuclear magnetic resonance imaging on the assessment of multiple sclerosis patients*. Semin Neurol. 1986 Mar;6(1):24-32.

[10] Ormerod IE, Miller DH, McDonald WI, Du Boulay EP, Rudge P, Kendall BE. *The role of NMR imaging in the assessment of multiple sclerosis and isolated neurological lesions. A quantitative study*. Brain. 1987 Dec;110(Pt 6): 1579-616.

[11] Isaac C, Li DK, Genton M, Jardine C, Grochowski E, Palmer M. *Multiple sclerosis: a serial study using MRI in relapsing patients*. Neurology. 1988 Oct;38(10):1511-5.

[12] Kappos L, Stadt D, Ratzka M, Keil W, Schneiderbanger-Grygier S, Heitzer T. *Magnetic resonance imaging in the evaluation of treatment in multiple sclerosis*. Neuroradiology. 1988;30(4):299-302.

[13] Willoughby EW, Grochowski E, Li DK, Oger J, Kastrukoff LF, Paty DW. *Serial magnetic resonance scanning in multiple sclerosis: a second prospective study in relapsing patients*. Ann Neurol. 1989 Jan;25(1):43-9.

[14] Montalban X, *CIS diagnostics and predictors of conversion to CDMS*. Multiple sclerosis and related disorders. 2014 Nov; 3(6).

[15] Stüber C, Pitt, D, Wang Y. *Iron in Multiple Sclerosis and Its Noninvasive Imaging with Quantitative Susceptibility Mapping*. International Journal of Molecular Sciences. 2016;17.

[16] Rouault TA, Cooperman S. *Brain iron metabolism*. Semin Pediatr Neurol. 2006 Sep;13(3):142-8.

[17] Hallgren B, Sourander P. *The effect of age on the non-haemin iron in the human brain*. J. Neurochem. 1958;3:41-51.

[18] Connor JR, Menzies SL, St. Martin SM, Mufson EJ. *Cellular distribution of transferrin, ferritin, and iron in normal and aged human brains*. J. Neurosci. Res. 1990; 27:595-611.

[19] Connor JR, Menzies SL. *Cellular management of iron in the brain*. J. Neurol. Sci. 1995;134:33-44.

[20] Zheng W, Monnot AD. *Regulation of brain iron and copper homeostasis by brain barrier systems: Implication in neurodegenerative diseases*. Pharmacol. Ther. 2012;133: 177-188

[21] Hallgren B, Sourander P. *The effect of age on the non-haemin iron in the human brain*. J. Neurochem. 1958;3:41-51.

[22] Fukunaga M, Li T, Van Gelderen P, De Zwart JA, Shmueli K, Yao B, Lee J, Maric D, Aronova MA, Zhang G. *Layer-specific variation of iron content in cerebral cortex as a source of MRI contrast*. Proc. Natl. Acad. Sci. 2010;107:3834-3839.

[23] Stüber C, Morawski M, Schäfer A, Labadie C, Wähnert M, Leuze C, Streicher M, Barapatre N, Reimann K, Geyer S. *Myelin and iron concentration in the human brain: A quantitative study of MRI contrast*. Neuroimage. 2014;93:95-106.

[24] Cairo G, Bernuzzi F, Recalcati S. *A precious metal: Iron, an essential nutrient for all cells.* Genes Nutr. 2006;1:25-39.

[25] Corna G, Campana L, Pignatti E, Castiglioni A, Tagliafico E, Bosurgi L, Campanella A, Brunelli S, Manfredi AA, Apostoli P. *Polarization dictates iron handling by inflammatory and alternatively activated macrophages*. Haematologica. 2010;95:1814-1822

[26] Recalcati S, Locati M, Marini A, Santambrogio P, Zaninotto F, De Pizzol M, Zammataro L, Girelli D, Cairo G. *Differential regulation of iron homeostasis during human macrophage polarized activation*. Eur. J. Immunol. 2010;40:824-835.

[27] Xiong S, She H, Takeuchi H, Han B, Engelhardt JF, Barton CH, Zandi E, Giulivi C, Tsukamoto H. *Signaling role of intracellular iron in NF-κB activation*. J. Biol. Chem. 2003;278:17646-17654.

[28] Chen L, Xiong S, She H, Lin SW, Wang J, Tsukamoto H. *Iron causes interactions of TAK1, p21ras, and phosphatidylinositol 3-kinase in caveolae to activate IκB kinase in hepatic macrophages*. J. Biol. Chem. 2007;282:5582-5588.

[29] Haider L, Simeonidou C, Steinberger G, Hametner S, Grigoriadis N, Deretzi G, Kovacs GG, Kutzelnigg A, Lassmann H, Frischer JM. *Multiple sclerosis deep grey matter: the relation between demyelination, neurodegeneration, inflammation and iron*. J. Neurol. Neurosurg. Psychiatry. 2014;85:1386-1395.

[30] Raz E, Branson B, Jensen JH, Bester M, Babb JS, Herbert J, Grossman RI. *Relationship between iron accumulation and white matter injury in multiple sclerosis: A case–control study*. J. Neurol. 2014;262:402-409.

[31] Stankiewicz J, Panter SS, Neema M, Arora A, Batt CE, Bakshi R. *Iron in chronic brain disorders: Imaging and neurotherapeutic implications*. Neurotherapeutics. 2007;4: 371-386.

[32] Boven LA, Van Meurs M, Van Zwam M, Wierenga-Wolf A, Hintzen RQ, Boot RG, Aerts JM, Amor S, Nieuwenhuis EE, Laman JD. *Myelin-laden macrophages are anti-inflammatory, consistent with foam cells in multiple sclerosis*. Brain. 2006;129:517-526.

[33] Taetzsch T, Levesque S, McGraw C, Brookins S, Luqa R, Bonini MG, Mason RP, Oh U, Block ML. *Redox regulation of NF-κB p50 and M1 polarization in microglia*. Glia. 2015;63:423-440.

[34] Hametner S, Wimmer I, Haider L, Pfeifenbring S, Brück W, Lassmann H. *Iron and neurodegeneration in the multiple sclerosis brain*. Ann. Neurol. 2013;74:848-861.

[35] Chen W, Gauthier SA, Gupta A, Comunale J, Liu T, Wang S, Pei M, Pitt D, Wang Y. *Quantitative susceptibility mapping of multiple sclerosis lesions at various ages.* Radiology. 2014;271:183-192.

[36] Gillen KM, Mubarak M, Nguyen TD, Pitt D. *Significance and In Vivo Detection of Iron-Laden Microglia in White Matter Multiple Sclerosis Lesions*. Front Immunol. 2018 Feb 19;9:255.

[37] Duyn JH, Schenck J. *Contributions to magnetic susceptibility of brain tissue*. NMR Biomed. 2017 Apr;30(4):10.

[38] Shmueli K, De Zwart JA, Van Gelderen P, Li TQ, Dodd SJ, Duyn JH. *Magnetic susceptibility mapping of brain tissue in vivo using MRI phase data.* Magn Reson Med. 2009 Dec;62(6):1510-22.

[39] Liu C, Wei H, Gong NJ, Cronin M, Dibb R, Decker K. *Quantitative Susceptibility Mapping: Contrast Mechanisms and Clinical Applications.* Tomography. 2015;1(1):3-17.

[40] Liu T, Spincemaille P, De Rochefort L, Kressler B, Wang Y. *Calculation of susceptibility through multiple orientation sampling (COSMOS): a method for conditioning the inverse problem from measured magnetic field map to susceptibility source image in MRI*. Magn Reson Med. 2009;61(1):196–204.

[41] Wharton S, Schäfer A, Bowtell R. *Susceptibility mapping in the human brain using threshold-based k-space division.* Magn Reson Med. 2010;63(5):1292– 1304.

[42] Barkhof F. *The clinico-radiological paradox in multiple sclerosis revisited*. Curr Opin Neurol. 2002;15(3):239–245.

[43] Al-Radaideh AM, Wharton SJ, Lim S-Y, Tench CR, Morgan PS, Bowtell RW. *Increased iron accumulation occurs in the earliest stages of demyelinating disease: an ultra-high field susceptibility mapping study in Clinically Isolated Syndrome*. Mult Scler. 2013;19(7):896–903.

[44] Blazejewska AI, Al-Radaideh AM, Wharton S, Lim SY, Bowtell RW, Constantinescu CS, Gowland PA. *Increase in the iron content of the substantia nigra and red nucleus in multiple sclerosis and clinically isolated syndrome: a 7 Tesla MRI study*. J Magn Reson Imaging. 2015;41(4):1065–1070.

[45] Rudko DA, Solovey I, Gati JS, Kremenchutzky M, Menon RS. *Multiple sclerosis: improved identification of disease-relevant changes in gray and white matter by using susceptibility-based MR imaging*. Radiology. 2014;272(3):851–864.

[46] Liu C, Li W, Tong KA, Yeom KW, Kuzminski S. *Susceptibility-weighted imaging and quantitative susceptibility mapping in the brain*. J Magn Reson Imaging. 2015 Jul;42(1):23-41.

[47] Schmidt P, Gaser C, Arsic M, Buck D, Förschler A, Berthele A, Hoshi M, Ilg R, Schmid VJ, Zimmer C, Hemmer B, Mühlau M. *An automated tool for detection of FLAIR-hyperintense white-matter lesions in Multiple Sclerosis*. Neuroimage. 2012 Feb 15;59(4):3774-83.

[48] Schmidt P, Pongratz V, Küster P, Meier D, Wuerfel J, Lukas C, Bellenberg B, Zipp F, Groppa S, Sämann PG, Weber F, Gaser C, Franke T, Bussas M, Kirschke J, Zimmer C, Hemmer B, Mühlau M. *Automated segmentation of changes in FLAIR-hyperintense white matter lesions in multiple sclerosis on serial magnetic resonance imaging*. Neuroimage Clin. 2019;23:101849.

[49] Rojas JI, Patrucco L, Miguez J, Cristiano E. *Brain atrophy in multiple sclerosis: therapeutic, cognitive and clinical impact.* Arq Neuropsiquiatr. 2016 Mar;74(3):235-43.

[50] Sastre-Garriga J, Pareto D, Rovira À. *Brain Atrophy in Multiple Sclerosis: Clinical Relevance and Technical Aspects.* Neuroimaging Clin N Am. 2017 May;27(2):289-300.

[51] Eshaghi A, Marinescu RV, Young AL, Firth NC, Prados F et al. *Progression of regional grey matter atrophy in multiple sclerosis.* Brain. 2018 Jun 1;141(6):1665-1677.

[52] Fisher E, Rudick RA, Simon JH, Cutter G, Baier M, Lee JC et al. *Eight-year follow-up study of brain atrophy in patients with MS.* Neurology. 2002;59(9):1412-20.

[53] Fisniku LK, Chard DT, Jackson JS, Anderson VM, Altmann DR, Miszkiel KA. *Gray matter atrophy is related to long-term disability in multiple sclerosis.* Ann Neurol. 2008;64(3):247-54.

[54] Amato MP, Hakiki B, Goretti B, Rossi F, Stromillo ML, Giorgio A. *Association of MRI metrics and cognitive impairment in radiologically isolated syndromes.* Neurology. 2012;78(5):309-14.

[55] Yaldizli O, Penner IK, Frontzek K, Naegelin Y, Amann M, Papadopoulou A. *The relationship between total and regional corpus callosum atrophy, cognitive impairment and fatigue in multiple sclerosis patients.* Mult Scler. 2013;20(3):356-64.

[56] Kurtzke JF. *Rating neurologic impairment in multiple sclerosis: an expanded disability status scale (EDSS).* Neurology. 1983 Nov;33(11):1444-52.

[57] Li W, Wu B, Liu C. *STI Suite: a Software Package for Quantitative Susceptibility Imaing.* Joint Annual Metting ISMRM-ESMRMB. 2013.

[58] Li W, Avram AV, Wu B, Xiao X, Liu C. *Integrated Laplacian-based phase unwrapping and background phase removal for quantitative susceptibility mapping.* NMR Biomed. 2014 Feb;27(2):219-27.

[59] Law MT, Traboulsee AL, Li DK, Carruthers RL, Freedman MS, Kolind SH, Tam R. *Machine learning in secondary progressive multiple sclerosis: an improved predictive model for short-term disability progression.* Mult Scler J Exp Transl Clin. 2019 Nov 6;5(4):2055217319885983.

[60] Mateos-Pérez JM, Dadar M, Lacalle-Aurioles M, Iturria-Medina Y, Zeighami Y, Evans AC. *Structural neuroimaging as clinical predictor: A review of machine learning applications.* Neuroimage Clin. 2018 Aug 10;20:506-522.

[61] Salat DH, Greve DN, Pacheco JL, Quinn BT, Helmer KG, Buckner RL, Fischl B. *Regional white matter volume differences in nondemented aging and Alzheimer's disease.* Neuroimage. 2009 Feb 15;44(4):1247-58.

[62] Vrenken H, Geurts JJ. *Gray and normal-appearing white matter in multiple sclerosis: an MRI perspective*. Expert Rev Neurother. 2007 Mar;7(3):271-9.

[63] Moll NM, Rietsch AM, Thomas S, Ransohoff AJ, Lee JC, Fox R, Chang A, Ransohoff RM, Fisher E. *Multiple sclerosis normal-appearing white matter: pathology-imaging correlations.* Ann Neurol. 2011 Nov;70(5):764-73.

[64] Nowacki P, Koziarska D, Masztalewicz M. *Microglia and astroglia proliferation within the normal appearing white matter in histologically active and inactive multiple sclerosis*. Folia Neuropathol. 2019;57(3):249-257.